

**Evidence of a Mesoscale Wave Phenomenon in the Lee of the  
Rocky Mountains**

by

R.A. Dirks, J.D. Mahlman, and Elmar R. Reiter

Technical Paper No. 115  
Department of Atmospheric Science  
Colorado State University  
Fort Collins, Colorado



**Department of  
Atmospheric Science**

Paper No. 115

EVIDENCE OF A MESOSCALE WAVE PHENOMENON  
IN THE LEE OF THE ROCKY MOUNTAINS

by  
R. A. Dirks, J. D. Mahlman, and Elmar R. Reiter

This report was prepared with support  
under Grant E-10-68G from the  
National Environmental Satellite Center, ESSA

Department of Atmospheric Science  
Colorado State University  
Fort Collins, Colorado

September 1967

Atmospheric Science Paper No. 115

ABSTRACT

Satellite photographs during the summer months frequently reveal a weather situation in which strong convective development is observed over the Rocky Mountains and several hundred kilometers to the east of the mountains, while the region immediately to the lee is essentially cloud free. It is proposed that an orographically induced mesoscale wave phenomenon may produce this situation. A dynamical model is developed which yields standing wave solutions of wavelength  $< 1000$  km for conditions of low mean wind speed and low thermal stability. Application of the model to the case of 20-21 July 1966 indicates a reasonable agreement between observation and theory; however, the sensitivity of the model to input parameters suggests that certain refinements need to be made. Further investigation will be necessary to determine the extent to which orographic influences are responsible for the generation of mesoscale systems.

## I. Introduction

Mesoscale systems (dimensions  $10^4$  -  $10^6$  m) have been studied with increasing emphasis during recent years, particularly with regard to severe storms. Important advances have been made through the efforts of the Thunderstorm Project and the National Severe Storms Project by employing a dense ground-base measurement network equipped with continuously recording instruments (Byers and Braham, 1949; Lee, 1962). In addition, regular upper air data were supplemented by radar observations and specially instrumented aircraft flights. In this way some of the more prominent mesoscale structures such as dew point fronts, the low-level jet, and squall lines have been explored successfully (McGuire, 1962; Bonner, 1966; Fujita, 1955). However, a major data gap still exists in the free atmosphere. On the average upper air stations are spaced over 300 km apart and for the detection and study of mesoscale systems this spatial resolution is generally inadequate. Meteorological satellites provide a valuable means of bridging this gap, especially so since early 1966 when satellite coverage has been made available over a given region several times a day.

In eastern Colorado, frequently during the summer, convective cloud and thunderstorm development is observed initially over the mountains beginning about mid-morning followed by afternoon development far to the east of the Continental Divide (100-500 km). The latter convective activity frequently develops into extensive squall lines which sometimes migrate eastward, persisting into the late night and early morning hours. Between these regions of convective development, a well-defined cloud free region is commonly observed immediately to the lee of the mountains. This gap is considerably larger than that suggested by lee-wave theory ( $\sim 10$  km), yet considerably smaller than the wave length of planetary disturbances (Scorer, 1949; Bolin, 1950).

On 20 July the cloud features in this belt exhibit a general cellular structure with several regions of more intense development. By 21 July the system has a more unified appearance in the television pictures. The infrared pictures taken 21 July, 0612 GMT and 0757 GMT (Fig. 5), indicate fairly distinct regions of pronounced development spaced on the order of 100 or 200 kilometers apart (scale distortion at the picture edges prevents an accurate estimation of the distances involved). Such spacing could possibly be interpreted as a succession of stationary mesoscale waves. Several such excessively bright regions appear along the cold front in Fig. 1, taken by Nimbus II HRIR, 20 July at 0645 GMT. These could conceivably result from the amplification of frontal activity due to the superposition of a mesoscale wave disturbance. The distribution of precipitation (Fig. 11) further supports the concept of aligned regions of more intense convective activity and also delineates the southern limit of the squall line in central Oklahoma.

The surface analysis for 22 July, 0600 GMT indicates the formation of a pre-cold front squall line in extreme western Kansas, as the front advances into the region. This squall line, unlike the pre-existing one, shows a definite relation to the cold front; however, it too may have been triggered by an orographically generated mesoscale wave. The presence of a mountain range certainly is not a necessary condition for squall development since it has long been known that such pre-frontal squall lines occur frequently in regions far removed from orographic influences (Newton, 1950). However, the fact that the line of thunderstorms considered here develops in the lee of the mountains in a region frequented by strong convective activity and hailfall, and also assumes an orientation nearly parallel to the mountains, suggests a certain orographic control in this formation. Infrared photography corresponding closely to the time of the surface analysis shows that intense development of the squall line has not yet occurred (Fig. 9, Nimbus HRIR photograph taken 22 July at 0724 GMT). Subsequent maps and photographs

illustrate the passage of the second cold front through the region under study; however, this time the extensive cloud cover does not reveal the distinct regions of pronounced development, and the cloud band in western Kansas does not exist after the frontal advance.

The Colorado State University Hail Project observed hailstorms in the late afternoon on both 20 and 21 July (Marwitz, 1967). In each case the storm was observed to develop over the mountains, producing hail immediately to the lee of the mountains as shown by asterisks in Fig. 11. Evidence of the storm on the 21st of July may be seen in Fig. 8 just northeast of the 105 longitude 40 latitude intersection. Both of these storms died out or deteriorated rapidly as they moved eastward. This fact lends further evidence that convective activity near, and to the lee of, the mountains is suppressed by mesoscale dynamical effects.

Upper air analyses reveal a short wave over the Great Plains which appears in both the temperature and height contours (Fig. 12). The persistence of this feature, shown on the maps of 19 July, 0000 GMT to 22 June, 0000 GMT, suggests a quasi-stationary nature of the disturbance. The assumption of a stationary wave phenomenon, on which the following dynamic model is based, thus appears justified. The analyses presented here, as well as the upper winds at levels below 500 mb, indicate a cyclonic circulation in the region of interest, whereas the large scale flow pattern over the western and central United States is generally anticyclonic. The jet stream influence is probably not significant since the region of maximum wind is located quite far to the north over the Dakotas and also has an anticyclonic curvature.

### III. Theoretical Model

Theoretical approaches to the formulation of mesoscale flow phenomena in terms of the fundamental dynamical equations have been few, primarily because such approaches had to be purely academic for lack of observational data. With the availability of cloud photographs taken at regular intervals over the same geographic area, one may now check a given theory against observational evidence provided by well-developed cloud systems.

Since mountain barriers are known to generate planetary waves (Bolin, 1950), as well as gravity waves of the shorter dimensions of lee waves (Scorer, 1949) and of clear air turbulence (Foltz, 1967; Reiter and Foltz, 1967), one may suspect that orographic obstacles can also serve as a source region for mesoscale disturbances. The region to the east of the Colorado Rockies, therefore, is of particular interest for the study of such flow phenomena. From previous investigations there is evidence available which documents that this orographic barrier is capable of producing mesoscale phenomena under certain conditions (Conover, 1960; Reiter, et al., 1965; Reiter and Mahlman, 1965; Chappell, 1967). These mesoscale waves apparently exhibit a quasi-horizontal character, at least qualitatively similar to synoptic-scale waves.

In most theoretical studies of atmospheric motion, the physical equations are scaled a priori in such manner that either the large scale waves or the gravitational waves are systematically eliminated. The justification for such scaling is based on the usually valid assumption that a discrete separation of scales exists between the micro- and macroscales in the atmosphere. However, as noted above, this may not be strictly true under certain atmospheric conditions. The intent of this chapter is to deal with flow processes in such manner that the basic physical equations do not eliminate this intermediate scale prior to the analysis.

In order that an analytical solution can be attained, the standard linearization procedure is employed in which the disturbed motion is a small perturbation on a well-defined mean flow. Since the theoretical model will be applied to the region east of the Rocky Mountains, we may assume that the waves generated by the mountain barrier will be stationary. It will be shown that the inclusion of this restraint acts to reduce the usual wave spectrum to a single wavelength which is uniquely defined in terms of characteristics of the basic current.

In order to simplify the problem without destroying the character of the physical problem, the following assumptions are employed:

- 1) The flow is hydrostatic, frictionless, and adiabatic;
- 2) The perturbation motion is assumed to be independent of the y coordinate;
- 3) The basic current possesses vertical, but no lateral wind shear;
- 4) In the continuity equation, horizontal density advection is assumed to be negligible relative to vertical density advection;
- 5) Static stability and vertical wind shear are assumed to be constant;
- 6) Although the mean wind speed and mean temperature are actually functions of height, whenever they appear in undifferentiated form, they are replaced by a suitable vertically averaged value. This mathematical expedient was first employed by Rossby (1939) and later by Charney (1947).
- 7) The basic current is assumed to be zonal with no mean y and z components;
- 8) The earth is assumed to be an infinite, rotating plane.

The fundamental equations used in this analysis are:

$$\frac{\partial u}{\partial t} + u \frac{\partial u}{\partial x} + w \frac{\partial u}{\partial z} + RT \frac{\partial \ln p}{\partial x} - fv = 0 \quad (1)$$

$$\frac{\partial v}{\partial t} + u \frac{\partial v}{\partial x} + w \frac{\partial v}{\partial z} + RT \frac{\partial \ln p}{\partial y} + fu = 0 \quad (2)$$

$$\frac{-g}{RT} - \frac{\partial \ln p}{\partial z} = 0 \quad (3)$$

$$\frac{\partial T}{\partial t} + u \frac{\partial T}{\partial x} + v \frac{\partial T}{\partial y} + w \left( \frac{\partial T}{\partial z} + \frac{g}{c_p} \right) = 0 \quad (4)$$

$$\frac{\partial u}{\partial x} + \frac{\partial v}{\partial y} + \frac{\partial w}{\partial z} + w \frac{\partial \ln \rho}{\partial z} = 0 \quad (5)$$

where t = time

x, y, z = Cartesian coordinate directions

R = gas constant for dry air

T = temperature

$\ln p$  = logarithm of pressure

f = Coriolis parameter

u, v, w = velocity components in x, y, and z directions

g = acceleration of gravity

$c_p$  = specific heat of dry air at constant pressure

$\rho$  = density

Eqs. (1-3) are the equations of motion, (4) is the thermodynamic equation, and (5) is the continuity equation. By writing the dependent variables of Eqs. (1-5) as the sum of a mean (bar) and a perturbation (prime) term, one obtains

$$\begin{aligned} u &= \bar{u} + u' \\ v &= v', \quad (\bar{v} = 0) \\ w &= w', \quad (\bar{w} = 0) \\ T &= \bar{T} + T' \\ \ln p &= (\overline{\ln p}) + (\ln p)' \end{aligned} \quad (6)$$

By substituting the definitions (6) into Eqs. (1-5) and assuming that products of perturbations are negligibly small, separate sets of equations for the mean and perturbation motion are obtained since the mean motion is satisfied independently.

The equations for the ground state are:

$$\bar{u} = - \frac{R\bar{T}}{f} \frac{\partial (\overline{\ln p})}{\partial y} \quad (7)$$

$$\frac{\partial (\overline{\ln p})}{\partial z} = \frac{-g}{R\bar{T}} \quad (8)$$

Thus, the ground state is completely specified by the geostrophic and hydrostatic equations. Combining Eqs. (7) and (8) gives the relation between the mean wind and the mean temperature field,

$$\frac{\partial \bar{u}}{\partial z} = \frac{-g}{f\bar{T}} \frac{\partial \bar{T}}{\partial y} - \frac{\bar{u}}{\bar{T}} \frac{\partial \bar{T}}{\partial z} \quad (9a)$$

or, to an excellent approximation for even large temperature lapse rates,

$$\frac{\partial \bar{u}}{\partial z} = \frac{-g}{f\bar{T}} \frac{\partial \bar{T}}{\partial y} \quad (9b)$$

This is the most common form of the thermal wind relationship.

The equations for the perturbed motion are given by

$$\frac{\partial u'}{\partial t} + \bar{u} \frac{\partial u'}{\partial x} + w' \frac{\partial \bar{u}}{\partial z} + R\bar{T} \frac{\partial (\overline{\ln p'})}{\partial x} - fv' = 0 \quad (10)$$

$$\frac{\partial v'}{\partial t} + \bar{u} \frac{\partial v'}{\partial x} + R\bar{T}' \frac{\partial (\overline{\ln p})}{\partial y} + fu' = 0 \quad (11)$$

$$\frac{\partial (\ln p)'}{\partial z} - \frac{gT'}{RT^2} = 0 \quad (12)$$

$$\frac{\partial T'}{\partial t} + \bar{u} \frac{\partial T'}{\partial x} + v' \frac{\partial \bar{T}}{\partial y} + w' \left( \frac{\partial \bar{T}}{\partial z} + \frac{g}{c_p} \right) = 0 \quad (13)$$

$$\frac{\partial u'}{\partial x} + \frac{\partial w'}{\partial z} + w' \frac{\partial (\overline{\ln \rho})}{\partial z} = 0 \quad (14)$$

Eq. (12) makes use of the expansion  $\frac{1}{T+T'} = \frac{1}{T} - \frac{T'}{T^2} + \dots$ , neglecting higher order terms.

In general, one may assume solutions for the linear Eqs. (10-14) of the form

$$\frac{u'}{A(z)} = \frac{w'}{B(z)} = \frac{v'}{C(z)} = \frac{(\ln p)'}{D(z)} = \frac{T'}{E(z)} = e^{i\mu(x-ct)} \quad (15)$$

where  $A(z)$ ,  $B(z)$ ,  $C(z)$ ,  $D(z)$ , and  $E(z)$  are possibly complex perturbation amplitudes;  $\mu$  is the wave number  $= \frac{2\pi}{L}$ ;  $L$  is the wavelength; and  $c$  is the phase speed which also may become complex. Since the perturbations are assumed to be orographically generated, hence stationary, no complex frequencies will be permitted. Consequently, in order that the physical perturbation quantities remain real, the perturbation amplitudes must also be real. In view of the realistic assumption that an orographic perturbation is produced at the ground and vanishes at great height, this suggests that the amplitude may be written in the form

$$A(z) = A_0 e^{nz} \quad (16)$$

where  $A_0$  is a constant, and  $n$  is a vertical damping coefficient-- assumed to be a negative, real number. With the use of this simplification, one may write the assumed solutions of Eqs. (15)

in the form

$$\frac{u'}{A_o} = \frac{w'}{B_o} = \frac{v'}{C_o} = \frac{(\ell n \rho)'}{D_o} = \frac{T'}{E_o} = e^{i\mu(x-ct) + nz} \quad (17)$$

A more complete justification for the use of this simplified assumed solution is presented in Appendix A. It is shown in this appendix, by use of the assumed solutions (15), that the perturbation amplitudes possess solutions of the same form as Eq. (16).

Now by substituting Eqs. (17) into Eqs. (10-14), one obtains

$$i\mu(\bar{u}-c)A_o + \frac{\partial \bar{u}}{\partial z} B_o + i\mu R\bar{T}D_o - fC_o = 0 \quad (18)$$

$$i\mu(\bar{u}-c)C_o + R \frac{\partial(\bar{\ell n p})}{\partial y} E_o + fA_o = 0 \quad (19)$$

$$nD_o - \frac{g}{R\bar{T}^2} E_o = 0 \quad (20)$$

$$i\mu(\bar{u}-c)E_o + \frac{\partial \bar{T}}{\partial y} C_o + \left( \frac{\partial \bar{T}}{\partial z} + \frac{g}{c_p} \right) B_o = 0 \quad (21)$$

$$i\mu A_o + nB_o + \frac{\partial \bar{\ell n \rho}}{\partial z} B_o = 0 \quad (22)$$

This is a system of linear, homogeneous algebraic equations. In order that non-trivial solutions exist, the determinant of the coefficients of Eqs. (18-22) must vanish. By substituting the ground state Eqs. (7) and (9b) and assuming (because of the stationary perturbation) that  $c = 0$ , solution of the determinant of the coefficients of Eqs. (18-22) for the stationary wavelength yields

$$L = \frac{2\pi}{f} \left\{ \frac{\bar{u} \left[ \bar{u}^{-2} n \left( n + \frac{\partial \bar{\ell n \rho}}{\partial z} \right) - \bar{u} n \frac{\partial \bar{u}}{\partial z} + \frac{g}{\bar{T}} \left( \frac{\partial \bar{T}}{\partial z} + \frac{g}{c_p} \right) \right]}{Q} \right\}^{1/2}, \quad (23)$$

where

$$Q = \bar{u}n \left( n + \frac{\partial \overline{\ln \rho}}{\partial z} \right) - \frac{\partial \bar{u}}{\partial z} \left( n + \frac{\partial \overline{\ln \rho}}{\partial z} \right) + \left( \frac{\partial \bar{u}}{\partial z} \right)^2 \frac{\bar{u}n}{g} - \bar{u}^2 \frac{\partial \bar{u}}{\partial z} \frac{n}{g} \left( n + \frac{\partial \overline{\ln \rho}}{\partial z} \right) - \frac{\bar{u}n}{\bar{T}} \left( \frac{\partial \bar{T}}{\partial z} + \frac{g}{c_p} \right) .$$

Since the wavelength is a positive real number, Eq. (23) allows only one simple wavelength in terms of the properties of the ground state variables and the damping coefficient  $n$ . A major difficulty arises in the evaluation of Eq. (23) because of the uncertainty in assessing the magnitude of  $n$ . However, an approximate range for  $n$  can be deduced on physical grounds. Fig. 13 gives the damping curves for various assumed values of  $n$  in the height range 0-10 km. A value of  $n = -10^{-4} \text{ m}^{-1}$  gives a perturbation intensity at 10 km which is 37% of the surface value. An  $n$  of  $-10^{-3} \text{ m}^{-1}$  produces virtually complete damping at 10 km and is reduced to 10% of the surface intensity at 2.3 km. Consequently, it may be deduced that the range  $-10^{-4} \text{ m}^{-1} < n < -10^{-3} \text{ m}^{-1}$  completely encompasses the allowable values of  $n$  in this particular model. Additional justification for this range of  $n$  is given in Appendix A.

Eq. (23) is rather difficult to evaluate in its present form. It can be simplified considerably if one notes from a simple scale analysis that, even for large values of  $\bar{u}$  and  $\frac{\partial \bar{u}}{\partial z}$ , the third and fourth terms in the denominator of Eq. (23) are always between two and three orders of magnitude smaller than the first and second terms. With this simplification Eq. (23) becomes

$$L = \frac{2\pi}{f} \left\{ \frac{\bar{u} \left[ \bar{u}^{-2} n \left( n + \frac{\partial \overline{\ln \rho}}{\partial z} \right) - \bar{u}n \frac{\partial \bar{u}}{\partial z} + \frac{g}{\bar{T}} \left( \frac{\partial \bar{T}}{\partial z} + \frac{g}{c_p} \right) \right]}{\left( n + \frac{\partial \overline{\ln \rho}}{\partial z} \right) \left( \bar{u}n - \frac{\partial \bar{u}}{\partial z} \right) - \frac{\bar{u}n}{\bar{T}} \left( \frac{\partial \bar{T}}{\partial z} + \frac{g}{c_p} \right)} \right\}^{1/2} . \quad (24)$$

#### IV. Evaluation of the Wavelength Equation

It is now of particular interest to determine from Eq. (24) what combination of input conditions acts to produce wavelengths in the mesoscale range. In order to simplify the interpretation of Eq. (24), it is assumed for all cases that  $\bar{T} = 250\text{K}$ ,  $f = 10^{-4} \text{sec}^{-1}$ ,  $\frac{\partial \ln \rho}{\partial z} = 10^{-4} \text{m}^{-1}$ , and that the wind shear ( $\frac{\partial u}{\partial z}$ ) can be directly related to the mean wind  $\bar{u}$ . This is accomplished by assuming that the mean wind is one-half the 10 km wind and that the wind shear may be simply expressed by twice the mean wind divided by the total distance 10 km. For example, a mean  $\bar{u}$  of  $10 \text{ m sec}^{-1}$  would possess a mean shear of  $2 \times 10^{-3} \text{sec}^{-1}$ ,  $\bar{u} = 15 \text{ m sec}^{-1}$  would have a shear of  $3 \times 10^{-3} \text{sec}^{-1}$ , etc. Strictly speaking, this is not completely accurate because, in this model, the mean wind does not vanish completely at the surface. However, the error committed is so small that its effect does not perceptibly alter the results.

With the above simplifications, Eq. (24) is such that the stationary wavelength  $L$  is determined by the mean wind field, the temperature lapse rate, and the value of the damping coefficient  $n$ . Solutions of Eq. (24) for various combinations of the above parameters are given in Fig. 14. In these figures the wavelength  $L$  is plotted against the stability  $\frac{\partial \bar{T}}{\partial z} + \frac{g}{c_p}$ . Each diagram is for a different given value of mean wind  $\bar{u}$ , and each curve in a given figure represents a constant specified value of  $n$ . One is now in a position to infer from Fig. 14 the conditions required for generation of mesoscale wavelengths. If one roughly considers the transition from meso- to synoptic-scale to be 1000 km, then Fig. 14 shows quite clearly that low mean wind speeds and small stability values ( $\frac{\partial \bar{T}}{\partial z} + \frac{g}{c_p}$ ) are highly favorable for the formation of wavelengths in the mesoscale region. It is also evident that larger negative values of  $n$  are more conducive to the generation of waves in the shorter scale. Conversely, high wind speeds and high stabilities do not permit formation of such meso-scale waves.

A further simplification of Eq. (24) can be achieved if, in the original perturbation Eqs. (10-14), the third term of Eq. (14) is omitted. This is equivalent to assuming that the flow is incompressible. In this case the equation for the wavelength is the same as Eq. (24) except that the  $\frac{\partial \overline{\ln \rho}}{\partial z}$  terms are absent. Fig. 15 gives the results for L in the same manner as in Fig. 14. It may be immediately seen that the results of Fig. 15 are very similar to Fig. 14, particularly for larger negative values of n. However, it is also evident that the predicted wavelength for the incompressible case is always longer than the wavelengths obtained for the compressible case. This result is analogous to the result obtained by Haurwitz (1931), which demonstrated that the wavelengths of billow clouds are always shorter for the condition of compressibility as compared with that obtained for an incompressible fluid.

Since the solution of Eq. (24) suggests very strongly that meso-scale waves will not form unless  $\bar{u}$  and  $\frac{\partial \bar{T}}{\partial z} + \frac{g}{c_p}$  are both quite small, it may be immediately inferred that only summertime flow conditions are at all favorable for the formation of these shorter waves. This inference is at least in qualitative agreement with observation since, in general, mesoscale phenomena occur most commonly east of the Rocky Mountains in the summer months.

## V. Comparison with Other Investigations

Only a very limited number of attempts have been made toward deducing the characteristics of waves in this intermediate region between the micro- and the synoptic-scale. Queney (1947), in a more general formulation, derives a differential equation for a pressure wave in this intermediate scale, but no attempt is made to deduce a wavelength for the case of a stationary orographic perturbation. He does, however, mention this possibility, and also alleges that these intermediate waves are controlled by the earth's rotation and the thermal stratification. This is in qualitative agreement with the result obtained here.

An admittedly crude analysis by Godske et al. (1957, p. 343) attempted to find a wavelength of maximum instability lying somewhere between that of inertial and shearing waves. However, since neither of the assumed regimes possessed any kinematic restraints in the original equations, it is difficult to see that much correspondence with reality could be expected. Moreover, the model employed in this paper is for a stable wave with zero propagation rate, while the analysis of Godske et al. attempted to find the wavelength of maximum instability. As a result of this, their result probably cannot be applied realistically here.

The results obtained in this paper are in quite satisfactory agreement with those presented by Kasahara (1966) for flow in a channel over a mountain barrier. Kasahara's investigation was a numerical integration of essentially the same equation set as Eqs. (1-5), but for the simplified case of the homogeneous, incompressible atmosphere. Furthermore, his analysis was for a circular obstacle rather than the infinite lateral mountain presented here. However, the results of his integrations show that the orographically induced wavelength in his model is only about one-third as long for the case of  $\bar{u} = 8 \text{ m sec}^{-1}$  as compared with the case of  $\bar{u} = 40 \text{ m sec}^{-1}$ . This result is in excellent agreement with those given in Figs. 14 and 15 and strongly suggests that the results from the linear analysis presented here may be tested against occurrence of such waves in the real atmosphere.

## VI. Comparison of Observation and Theory

The model proposed in the foregoing chapter predicts the generation of mesoscale waves only under very limited conditions--very low stability and light winds--and thus is most applicable to summer convective systems under orographic control. The strong circulation patterns associated with well-defined stable air masses during winter give solutions of a much larger scale (wavelengths in the order of

1000-3000 km), i. e., on the cyclone or synoptic scale. This is readily supported by the fact that wintertime synoptic features are dominated by large cyclones and anticyclones. The summer systems are much weaker (at least in total energy) and not nearly as well-defined, occurring mainly as weak frontal disturbances, squall lines, and clusters of thunderstorms. The effect of the weak large-scale circulation, thus, is readily over-ruled by regional mesoscale features as illustrated during July 1966.

Tropospheric data from the Denver soundings for 20-22 July may be applied to the theoretical model in order to test its applicability to a real atmosphere. The not uncommon occurrence of a near adiabatic lapse rate up to 500 or 550 mb at Denver during the summer, as shown in Fig. 16, provides the low thermal stability needed for the generation of mesoscale waves. This condition may also be met by a moist adiabatic ascent in a very moist atmosphere. The light wind conditions required for a mesoscale wave formation are also characteristic throughout this time period. Using only the westerly component of the wind field further reduces the wavelength obtained. (This is certainly valid due to the north-south orientation of the mountain range.)

Values of input parameters, as obtained from the Denver soundings, and computed wavelength are given in Table I. Since the model only allows for a linear vertical wind shear, this was estimated by the best linear fit to a vertical plot of the westerly component of the wind at Denver. The parameters were calculated between the surface (or surface inversion layer)  $ht_L$  and a mid-tropospheric level  $ht_U$ . This upper boundary was usually chosen as the discontinuity in the temperature field frequently found in summer conditions between 500 and 600 mb (see Fig. 16). When this discontinuity was not present, the 500 mb level was arbitrarily chosen as the upper boundary. Since the mountain

barrier reaches a maximum level of about 700 mb, it is reasonable to assume that the structure of the perturbation field is mainly determined by the features of the lower half of the troposphere. The mean wind value was determined as the mid-point of the linear wind profile. The temperature lapse rate was estimated by the difference between the boundary temperatures over the thickness of the layer. A value of  $n = -0.3 \times 10^{-3} \text{ m}^{-1}$  was used, the justification for which is given in Appendix A. A reasonable value of  $\frac{\partial \ln \rho}{\partial z}$  was assumed to be  $-0.1 \times 10^{-3} \text{ m}^{-1}$ .

TABLE I

Date	Time (GMT)	ht <sub>L</sub> (km)	ht <sub>U</sub> (km)	$\bar{T}$ (°K)	$\partial T/\partial z$ (°K/km)	$\bar{u}$ (m/s)	$\partial u/\partial z$ (m/s/km)	L <sub>c</sub> (km)
					moist adiabatic			
20	00	2.7	4.6	-		4.0	3.1	255
	12	2.3	4.5	260	6.02	2.5	2.3	1090
21	00	1.6	5.0	255	8.92	4.0	1.8	710
	12	2.4	5.4	265	8.15	1.0	-2.3	imag.

Results of these computations give a range of wavelengths from 200-1100 km which correspond favorably to the 500-600 km estimated from the satellite and precipitation data. The precision of these computations is greatly restricted because they are based on a single sounding in which local perturbation quantities may overshadow the mean regional conditions which determine the wave properties. It would probably be better to use the average of three or four soundings; however, the nearest stations (Grand Junction, North Platte, or Dodge City) are too far away to characterize the conditions found in the region of the mesoscale system. Also, the time scale (12 hours) is probably too large in most cases to allow the use of the

average of several successive soundings, even under quasi-stationary upper-flow conditions. Time-averaging might give a better approximation of mean conditions than the space-average of neighboring stations. An average of the condition for the first three times given in Table I was used to compute a mean wavelength. Due to the persistence and stationary character of this particular system, a reasonable average wavelength of 925 km was thus determined. The negative shearing term at 21 July, 12 GMT, does not appear to be applicable to the model. It is also questioned whether the negative shear represents the mean flow conditions.

The dominance of the stability term in Eq. (24) is very evident from Fig. 14 in the previous chapter. This can also be easily seen from an order of magnitude calculation of the terms under the radical in the wavelength equation, Eq. (24). Assuming the following characteristic values:  $\bar{u} = 5 \text{ m/s}$ ,  $\partial u/\partial z = 1.0 \times 10^{-3} \text{ sec}^{-1}$ ,  $\bar{T} = 270 \text{ deg}$ ,  $\partial T/\partial z = 7.8 \times 10^{-3} \text{ deg/m}$ ,  $n = -0.3 \times 10^{-3}$ ,  $\partial \ln \rho/\partial z = -0.1 \times 10^{-3}$ , the radical terms then give:  $\frac{3.0 + 1.5 + 72.6}{.12 + .08 + .002}$ . The other terms in the numerator become significant only for near adiabatic conditions. The second term in the denominator may be large for conditions of large wind shear associated with a low mean wind component normal to the mountain range. The first term in the denominator is essentially a constant, the third term is generally negligible. Similar conclusions may be drawn from Fig. 14.

The rather sensitive dependence of wavelength on low stability values is clearly seen in Fig. 14. For example, looking at Fig. 14 for 5 m/s, a stability value of  $0.1 \times 10^{-3}$  and  $n = -0.3 \times 10^{-3}$  gives a wavelength of about 425 km, while a stability value of  $0.2 \times 10^{-3}$  yields a wavelength of about 525 km. Furthermore, an adiabatic lapse condition would give a wavelength of 300 km. Since lapse rate variations of a single sounding from actual mean conditions may be of a larger

magnitude than the values considered above, the computed wavelengths may be subject to considerable errors.

Wavelength estimates from satellite photographs or from wind field analyses made from the standard network are also subject to errors of similar magnitude. The above estimates of wavelength from satellite photographs assume a mesoscale ridge to be present over the Continental Divide, with a region of maximum convective development occurring at  $3/4$  of a wavelength downstream. This is in analogy to the region of maximum upper divergence found in planetary waves (Petterssen, 1956, p. 330). It is not unreasonable to assume that the same divergence distribution would apply to a mesoscale system as well.

It should be stated that the theoretical model in its present form is useful for indicating the probable existence or non-existence of mesoscale waves, but it is not adequate for accurately determining the wavelengths produced. It will be necessary to revise the model in order to make it less sensitive to the estimated input data, or else the input data will have to be more accurately determined.

Detailed wind analyses may, at times, reveal mesoscale wave features. An example is given by an analysis of the flow patterns for 8-9 May 1962 when a well-defined, slow-moving, mesoscale wave appears over the Great Plains (Fig. 17). It should be noted that this wave became evident only after pilot-balloon data were added to the information supplied by the standard radiosonde network (Reiter and Mahlman, 1965). This illustrates the inadequate resolution of the existing upper air network for the study of mesoscale phenomena. Application of the synoptic parameters from the Denver sounding yielded solutions in the range of 400-1400 km. Estimates from the wind analysis suggest a 800-1000 km wavelength. Unfortunately, no satellite data were available for this time period so that associated

cloud patterns and cloud-free regions could not be clearly observed. Precipitation data also favorably supports the wind analysis where heavy precipitation is found 700-800 km east of the Continental Divide (as seen in Fig. 18).

Unfortunately, the presently available wind information from the free atmosphere lacks the resolution of the cloud information provided by the weather satellite system. Even the combined use of radiosonde and pilot balloon network often has incomplete or missing data as a result of adverse weather in the mesoscale system under study. Heavy rainfall associated with squall lines or thunderstorms may prevent tracking of radiosonde or pilot balloons. Furthermore, local inflow into, and outflow from convective systems, may obscure the larger mesoscale circulation.

Although winds cannot be sensed directly from satellites as yet, ATS (stationary satellites) systems might provide enough resolution in the time scale so that considerable wind information could be inferred from the motion and development of cloud features. The levels in the atmosphere for which these motions are characteristic might, furthermore, be estimated in conjunction with high resolution infrared measurements.

## VII. Conclusions

Observational evidence of the orographic influence in the mesoscale region of the spectrum of atmospheric motions has been presented. Data from ESSA and Nimbus satellites is instrumental in detecting such mesoscale mountain influences on a systematic basis. These data may be used effectively in filling the gap between the capabilities of a single station ground observer and of the existing upper air network.

A theoretical model has been developed which explains the occurrence of mesoscale systems, but additional improvement is necessary to eliminate extreme sensitivity of the model to crudely estimated atmospheric input parameters, particularly the stability.

Mesoscale phenomena of this type deserve considerably more attention. A better understanding of these phenomena would provide more accurate short-term forecasting capability of severe weather occurrences to the lee of the Rocky Mountains and over the Great Plains. Orographic control immediately to the lee of the Rocky Mountains will have to be considered as an important factor in severe weather development east of the mountains. Further detailed investigations will be necessary to establish the extent to which a large orographic barrier is capable of modifying atmospheric structure and flow patterns in the meso-scale range.

#### Acknowledgements

The research reported in this paper has been conducted under Weather Bureau Grant E-10-68G. The computer facility of the National Center for Atmospheric Research has made available free computer time to this project.

REFERENCES

- Bolin, B., 1950: On the influence of the earth's orography on the general character of the westerlies. Tellus, 2, 184-195.
- Bonner, W. D., 1966: Case study of thunderstorm activity in relation to the low-level jet. Monthly Weather Review, 94, 167-178.
- Byers, H. and R. Braham, 1949: The Thunderstorm. U. S. Government Printing Office, Washington, D. C., 287 pp.
- Chappell, C., 1967: Personal communication.
- Charney, J. G., 1947: The dynamics of long waves in a baroclinic westerly current. Journal of Meteorology, 4, 135-162.
- Conover, J. H., 1960: Cirrus patterns and related air motions near the jet stream as derived by photography. Journal of Meteorology, 17, 532-546.
- Foltz, H. P., 1967: Prediction of clear air turbulence. Atmospheric Science Paper No. 106, Colorado State University, 145 pp.
- Fujita, T., 1955: Results of detailed synoptic studies of squall lines. Tellus, 7, 405-436.
- Godske, C. L., T. Bergeron, J. Bjerknes, and R. C. Bundgaard, 1957: Dynamical Meteorology and Weather Forecasting. American Meteorological Society and Carnegie Institution, 800 pp.
- Haurwitz, B., 1931: Wogenwolken und Luftwogen. Meteorologischen Zeitschrift, 12, 483-484.
- Kasahara, A., 1966: The dynamical influence of orography on the large scale motion of the atmosphere. Journal of the Atmospheric Sciences, 23, 259-271.
- Lee, J. T., 1962: A summary of field operations and data collection by the National Severe Storms Project in spring 1961. National Severe Storms Project Report No. 5, 47 pp.
- McGuire, E. L., 1962: The vertical structure of three dry lines as revealed by aircraft traverses. National Severe Storms Project Report No. 7, 10 pp.
- Marwitz, J., 1967: Personal communication.

- Newton, C. W., 1950: Structure and mechanism of the prefrontal squall line. Journal of Meteorology, 7, 210-222.
- Petterssen, S., 1956: Weather Analysis and Forecasting, Volume 1, 2nd Edition. McGraw-Hill Book Co., Inc., New York, 267 pp.
- Queney, P., 1947: A theoretical study of the perturbations of a rectilinear or zonal atmospheric current. Tropopause waves. Unpublished Manuscript, Institute for Advanced Study, Princeton, Jersey, 50 pp.
- Reiter, E. R., D. W. Beran, J. D. Mahlman, and G. Wooldridge, 1965: Effect of large mountain ranges on atmospheric flow patterns as seen from TIROS satellites. Atmospheric Science Technical Paper No. 69, Colorado State University, 1-53.
- \_\_\_\_\_, and H. P. Foltz, 1967: The prediction of clear air turbulence over mountainous terrain. AIAA Paper No. 67-184, presented at the 5th Aerospace Science Meeting, New York, January 23-26, 1967, 9 pp.
- \_\_\_\_\_, and J. D. Mahlman, 1965: Heavy iodine-131 fallout over the midwestern United States, May 1962. Atmospheric Science Technical Paper No. 70, Colorado State University, 1-53.
- Rossby, C. -G., and Collaborators, 1939: Relation between variations in the intensity of the zonal circulation of the atmosphere and the displacements of the semi-permanent centers of action. Journal of Marine Research, 2, 38-55.
- Scorer, R. S., 1949: Theory of airflow over mountains. Quarterly Journal of the Royal Meteorological Society, 75, 41-56.

Appendix A

In Part III of this paper it was argued that, for the stable perturbation equations under the boundary condition that an orographic perturbation must vanish at infinite height, the perturbation amplitude may be written in the form  $\text{const} \times e^{nz}$ . It is the intent of this section to provide a more rigorous justification for the use of this form of the perturbation amplitude. This will be accomplished by assuming the more general solution for the perturbations and solving for the form of the perturbation amplitude.

The fundamental equation set will, as before, be Eqs. (10-14). However, this time the assumed solutions will be of the more general form of Eqs. (15)

$$\frac{u'}{A(z)} = \frac{w'}{B(z)} = \frac{v'}{C(z)} = \frac{(\ln p)'}{D(z)} = \frac{T'}{E(z)} = e^{i\mu(x-ct)}. \quad (15)$$

By substitution of the assumed solutions (15) into Eqs. (10-14), one obtains the following equation set

$$i\mu(\bar{u}-c)A + \frac{\partial \bar{u}}{\partial z} B + i\mu R\bar{T}D - fC = 0 \quad (A-1)$$

$$i\mu(u-c)C - \frac{f\bar{u}}{\bar{T}} E + fA = 0 \quad (A-2)$$

$$\frac{dD}{dz} - \frac{g}{R\bar{T}^2} E = 0 \quad (A-3)$$

$$i\mu(\bar{u}-c)E + \frac{\partial \bar{T}}{\partial y} C + \left( \frac{\partial \bar{T}}{\partial z} + \frac{g}{c_p} \right) B \quad (A-4)$$

$$i\mu A + \frac{dB}{dz} + \frac{\partial(\overline{\ln \rho})}{\partial z} B = 0 \quad (A-5)$$

Eqs. (A1-A5) are a set of ordinary differential equations in terms of the perturbation amplitudes. Again, the mathematical expedient of Charney (1947) is utilized; whenever the mean wind speed and mean temperature appear in undifferentiated form, they are replaced by a representative mean value. By a very lengthy process of substitution and cross-differentiation, Eqs. (A1-A5) can be reduced to a second order differential equation in terms of the single unknown B

$$\left[ (\bar{u}-c) - \frac{f^2}{a^*} \right] \frac{d^2 B}{dz^2} + \left[ (\bar{u}-c) \frac{\partial \bar{\ln \rho}}{\partial z} + \frac{f^2 \frac{\partial \bar{u}}{\partial z}}{(\bar{u}-c) a^*} + \frac{f b^*}{a^*} + \frac{f^2 \dot{a}^*}{a^{2*}} \right] \frac{dB}{dz} + \quad (A-6)$$

$$\left[ \frac{\partial \bar{u}}{\partial z} \frac{\partial \bar{\ln \rho}}{\partial z} - \frac{f \frac{\partial \bar{u}}{\partial z} b^*}{(\bar{u}-c) a^*} + \frac{g \left( \frac{\partial \bar{T}}{\partial z} + \frac{g}{c_p} \right)}{\bar{T} (\bar{u}-c)} + \frac{f b^*}{a^*} - \frac{f \dot{a}^* b^*}{a^{2*}} \right] B = 0$$

where  $a^* = \mu (\bar{u}-c) + \frac{f \bar{u}}{g (\bar{u}-c)} \frac{\partial \bar{u}}{\partial z}$  (A-7)

$$b^* = f \left[ \frac{1}{\bar{T}} \frac{\bar{u}}{(\bar{u}-c)} \left( \frac{\partial \bar{T}}{\partial z} + \frac{g}{c_p} \right) - \frac{\partial \bar{\ln \rho}}{\partial z} \right] , \quad (A-8)$$

$$\dot{a}^* \equiv \frac{da^*}{dz} , \text{ and} \quad (A-9)$$

$$\dot{b}^* \equiv \frac{db^*}{dz} . \quad (A-10)$$

Eq. (A-6) is to be solved employing the single boundary condition  $B(\infty) = 0$ . In analogy with the more simplified approach in Part III it will be specified that  $c = 0$ , since the orographic perturbation is stationary in nature. As before, this procedure yields a single

wavelength in terms of the ground state parameters. For the case of  $c = 0$ , consider the following definitions:

$$\alpha \equiv \bar{u} - \frac{f^2}{a_1^*} \quad (\text{A-11})$$

$$\beta \equiv \bar{u} \frac{\partial \overline{\ln \rho}}{\partial z} + \frac{f^2 \frac{\partial \bar{u}}{\partial z}}{\bar{u} a_1^*} + \frac{f b_1^*}{a_1^*} + \frac{f^2 \dot{a}_1^*}{a_1^{2*}} \quad (\text{A-12})$$

$$\gamma \equiv \frac{\partial \bar{u}}{\partial z} \frac{\partial \overline{\ln \rho}}{\partial z} - \frac{f \frac{\partial \bar{u}}{\partial z} b_1^*}{\bar{u} a_1^*} + \frac{g \left( \frac{\partial \bar{T}}{\partial z} + \frac{g}{c_p} \right)}{\bar{T} \bar{u}} + \frac{f \dot{b}_1^*}{a_1^*} - \frac{f \dot{a}_1^* b_1^*}{a_1^{2*}} \quad (\text{A-13})$$

$$a_1^* \equiv \mu \bar{u} + \frac{f}{g} \frac{\partial \bar{u}}{\partial z} \quad (\text{A-14})$$

$$b_1^* \equiv f \left[ \frac{1}{\bar{T}} \left( \frac{\partial \bar{T}}{\partial z} + \frac{g}{c_p} \right) - \frac{\partial \overline{\ln \rho}}{\partial z} \right] \quad (\text{A-15})$$

$$\dot{a}_1^* \equiv \frac{d a_1^*}{d z} \quad (\text{A-16})$$

$$\dot{b}_1^* \equiv \frac{d b_1^*}{d z} \quad (\text{A-17})$$

With the above definitions Eq. (A-6) can now be written in the form

$$\alpha \frac{d^2 B}{dz^2} + \beta \frac{dB}{dz} + \gamma B = 0 \quad (\text{A-18})$$

Because of the method of regarding the ground state parameters as being effectively constant when appearing in undifferentiated form,

as long as a suitable mean level is chosen, Eq. (A-18) may be considered to be a linear second order differential equation with constant coefficients  $\alpha$ ,  $\beta$ , and  $\gamma$ . A general solution of Eq. (A-18) is

$$B(z) = K_1 \exp \left[ \frac{-\beta}{2\alpha} + \sqrt{\frac{\beta^2}{4\alpha^2} - \frac{\gamma}{\alpha}} \right] z + K_2 \exp \left[ \frac{-\beta}{2\alpha} - \sqrt{\frac{\beta^2}{4\alpha^2} - \frac{\gamma}{\alpha}} \right] z \quad (\text{A-19})$$

where  $K_1$  and  $K_2$  are arbitrary constants.

A particular solution of Eq. (A-19) can be obtained by employing the upper boundary condition  $B(\infty) = 0$ . It is difficult to apply this boundary condition immediately because the complicated nature of the bracketed terms does not readily permit identification of their respective algebraic signs. A way to circumvent this difficulty is to assign values of the ground state variables which indicated formation of wavelengths in the mesoscale range, and then evaluate the bracketed quantities of Eq. (A-19) in terms of sign and magnitude.

In line with this procedure the following values were selected:

$$\bar{u} = 10 \text{ m sec}^{-1}; f = 10^{-4} \text{ sec}^{-1}; \frac{\partial \bar{\ln \rho}}{\partial z} = -10^{-4} \text{ m}^{-1}; \bar{T} = 250 \text{ deg};$$

$$\frac{\partial \bar{T}}{\partial z} + \frac{g}{c_p} = 1 \times 10^{-3} \text{ deg m}^{-1}; L = 10^6 \text{ m}; \text{ and } \frac{\partial \bar{u}}{\partial z} = 2 \times 10^{-3} \text{ sec}^{-1}.$$

This gives the values for the derived quantities of:  $a_1^* \approx 39.5 \times 10^{-11} \text{ m}^{-1} \text{ sec}^{-1}$ ;  $a_1^* \approx .79 \times 10^{-13} \text{ m}^{-2} \text{ sec}^{-1}$ ;  $b^* \approx 1 \times 10^{-8} \text{ m}^{-1} \text{ sec}^{-1}$ ;  $b^* \approx 36 \times 10^{-14} \text{ m}^{-2} \text{ sec}^{-1}$ ;  $\alpha \approx 15.4 \text{ m sec}^{-1}$ ;  $\beta \approx 8.6 \times 10^{-3} \text{ sec}^{-1}$ ; and  $\gamma \approx 3.3 \times 10^{-6} \text{ m}^{-1} \text{ sec}^{-1}$ . By substitution of these numerical values Eq. (A-19) becomes to an excellent approximation:

$$B(z) \approx K_1 e^{+8.2 \times 10^{-4} z} + K_2 e^{-2.6 \times 10^{-4} z} \quad (\text{A-20})$$

Now if the upper boundary condition  $B(\infty) = 0$  is substituted into Eq. (A-20), to reject the positive root,  $K_1$  must = 0, and the form of B for the problem studied here is

$$B(z) = K_2 \exp \left[ \frac{-\beta}{2\alpha} - \sqrt{\frac{\beta^2}{4\alpha^2} - \frac{\gamma}{\alpha}} \right] z . \quad (\text{A-21})$$

For the numerical values assumed above

$$B(z) \approx K_2 e^{-2.6 \times 10^{-4} z} . \quad (\text{A-22})$$

It may be readily seen that the form of Eq. (A-21) is identical in form to that of the assumed form of the perturbation amplitude given in Eq. (16) if one is permitted to write

$$n = \frac{-\beta}{2\alpha} - \sqrt{\frac{\beta^2}{4\alpha^2} - \frac{\gamma}{\alpha}} .$$

As a consequence of this analysis, n is seen to be a very complicated function of the ground state parameters. For a given set of ground state parameters, n is a constant value. However, if the ground state conditions are changed, then n itself must change. Thus, contrary to the implications of Figs. 14 and 15, n may not be varied arbitrarily in this problem, but in actuality changes with the ground state conditions.

On the other hand, this does not negate the value of Figs. 14 and 15. This analysis merely suggests a more restricted range of acceptable n values, and as a result, probably more accurate values of stationary wavelength.

A check can be made on the equivalence of the two approaches outlined here by reading the value of n from Fig. 14 for the above

employed ground state parameters. This graph suggests a value of  $n$  of  $-2.9 \times 10^{-4} \text{ m}^{-1}$  for these conditions while the above analysis gives an approximate value of  $n \approx -2.6 \times 10^{-4} \text{ m}^{-1}$ . In view of the original uncertainty in determining a reasonable  $n$  value, this agreement is striking and suggests that the first approach may be employed with a high degree of confidence.

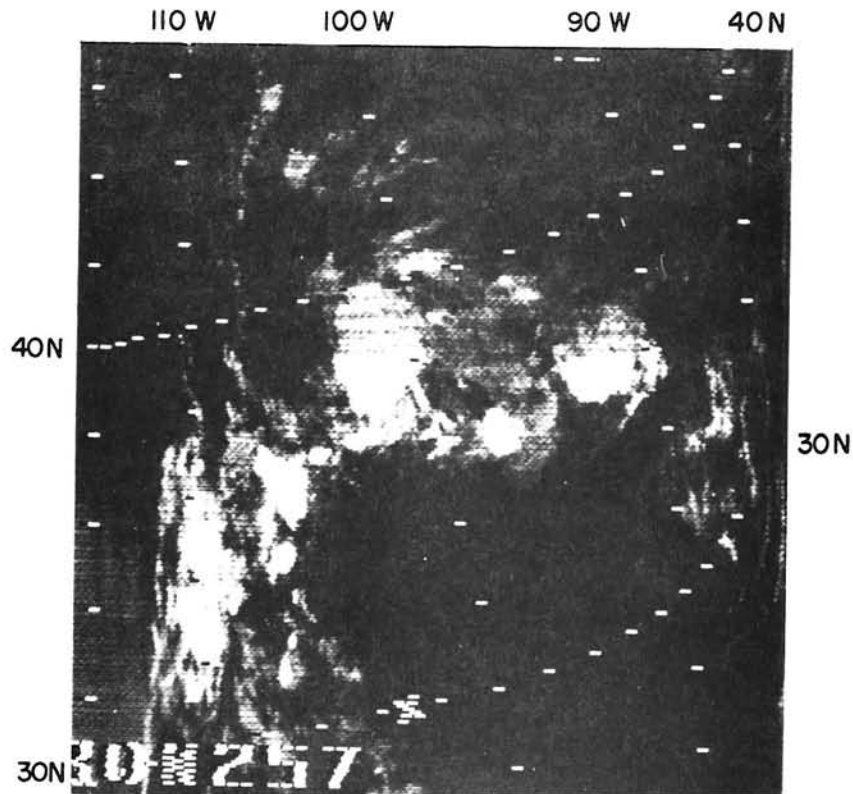


FIG. 1. Nimbus II HRIR (high resolution infrared radiometer), orbit 878, 20 July 1966, approximately 0645 GMT.

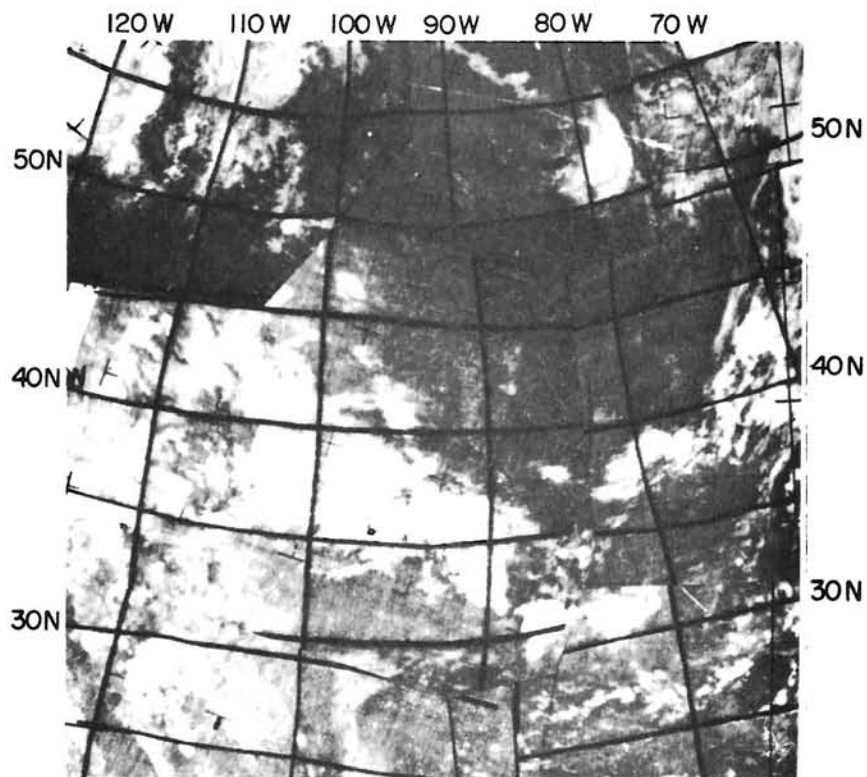


FIG. 2. ESSA II APT (automatic picture transmission) composite, orbit 1802, 20 July 1966, approximately 1533 GMT.

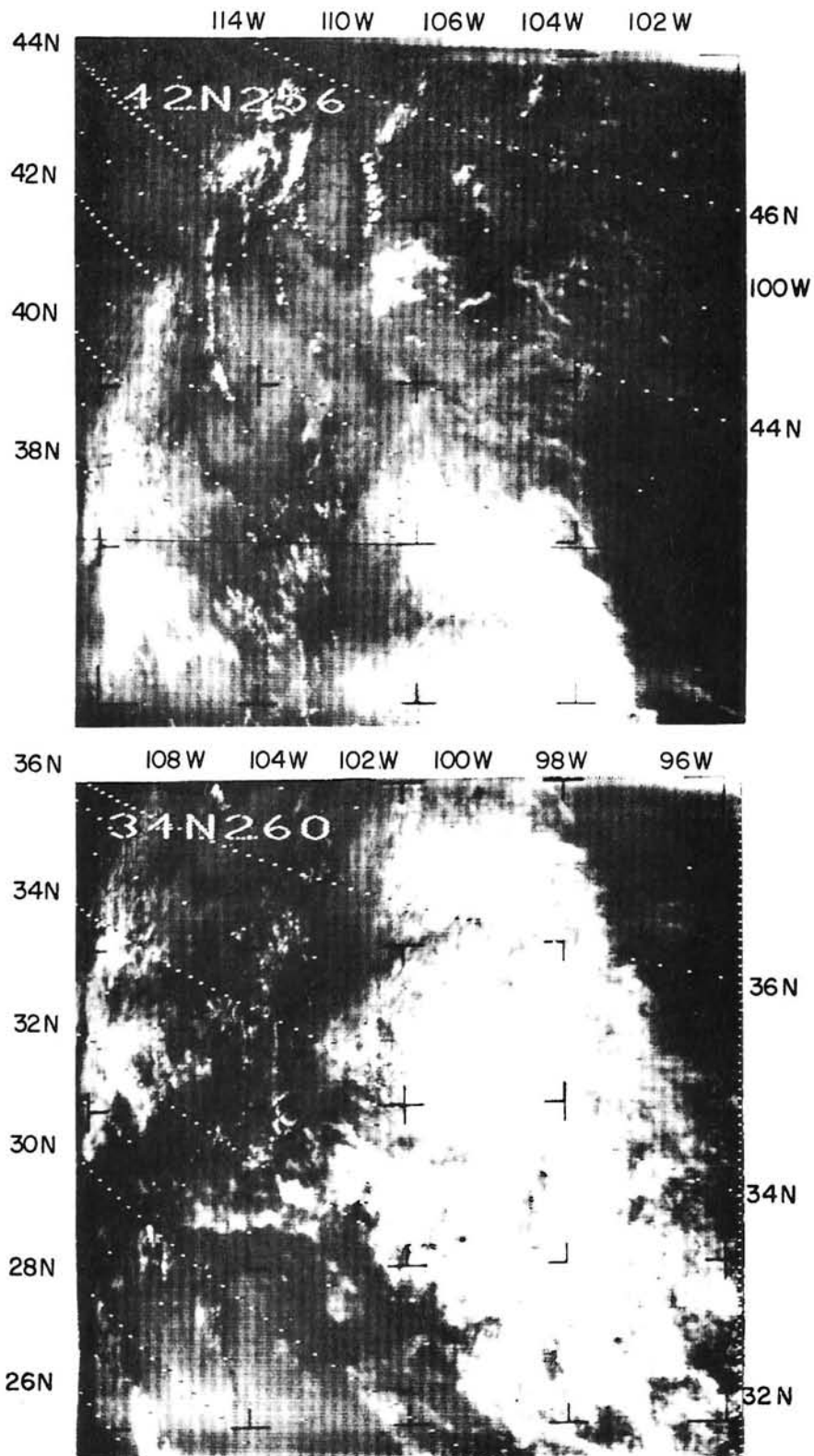


FIG. 3. Nimbus II AVCS (advanced vidicon camera system), orbit 884, camera 1, frames 78 and 79, 20 July 1966, 1705 GMT.

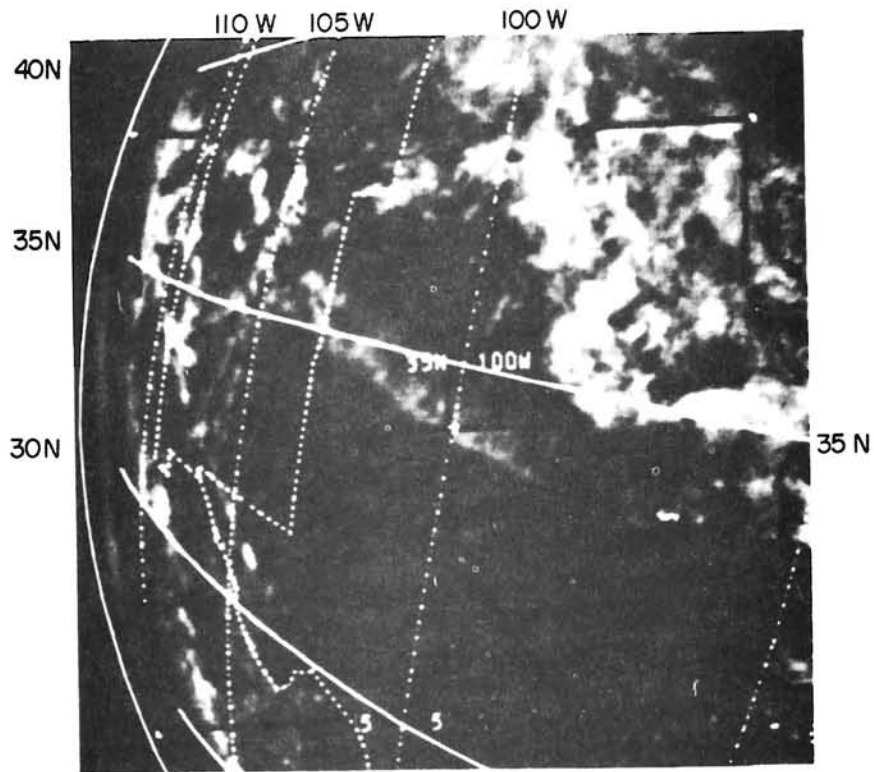
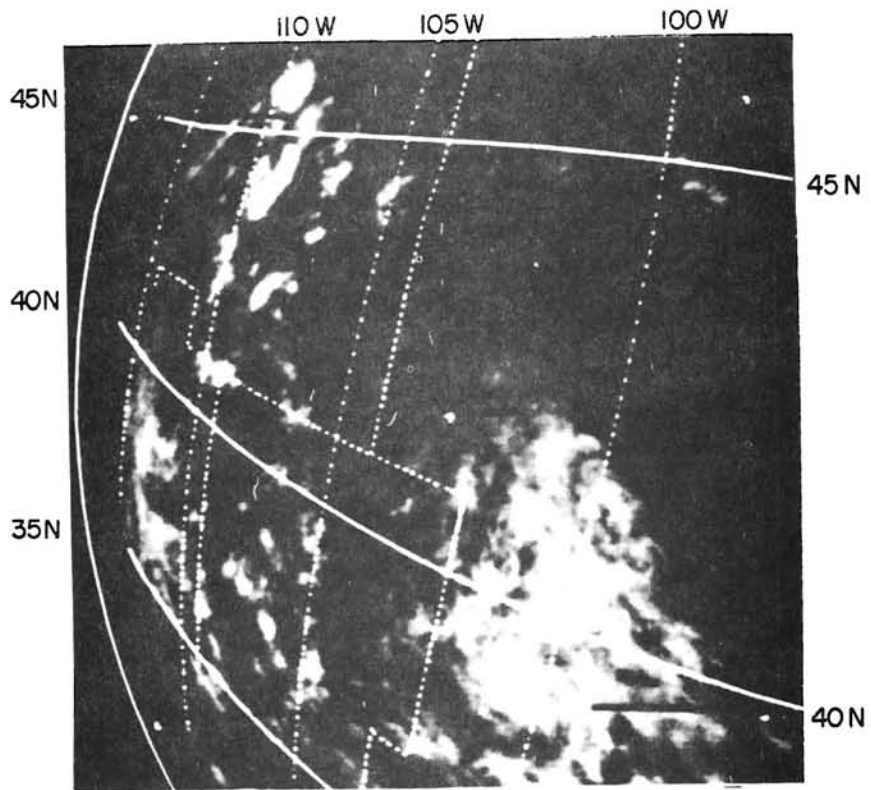


FIG. 4. ESSA I VCS (vidicon camera system), orbit 2403, camera 2, frames 3 and 4, 20 July 1966, 1934 GMT.

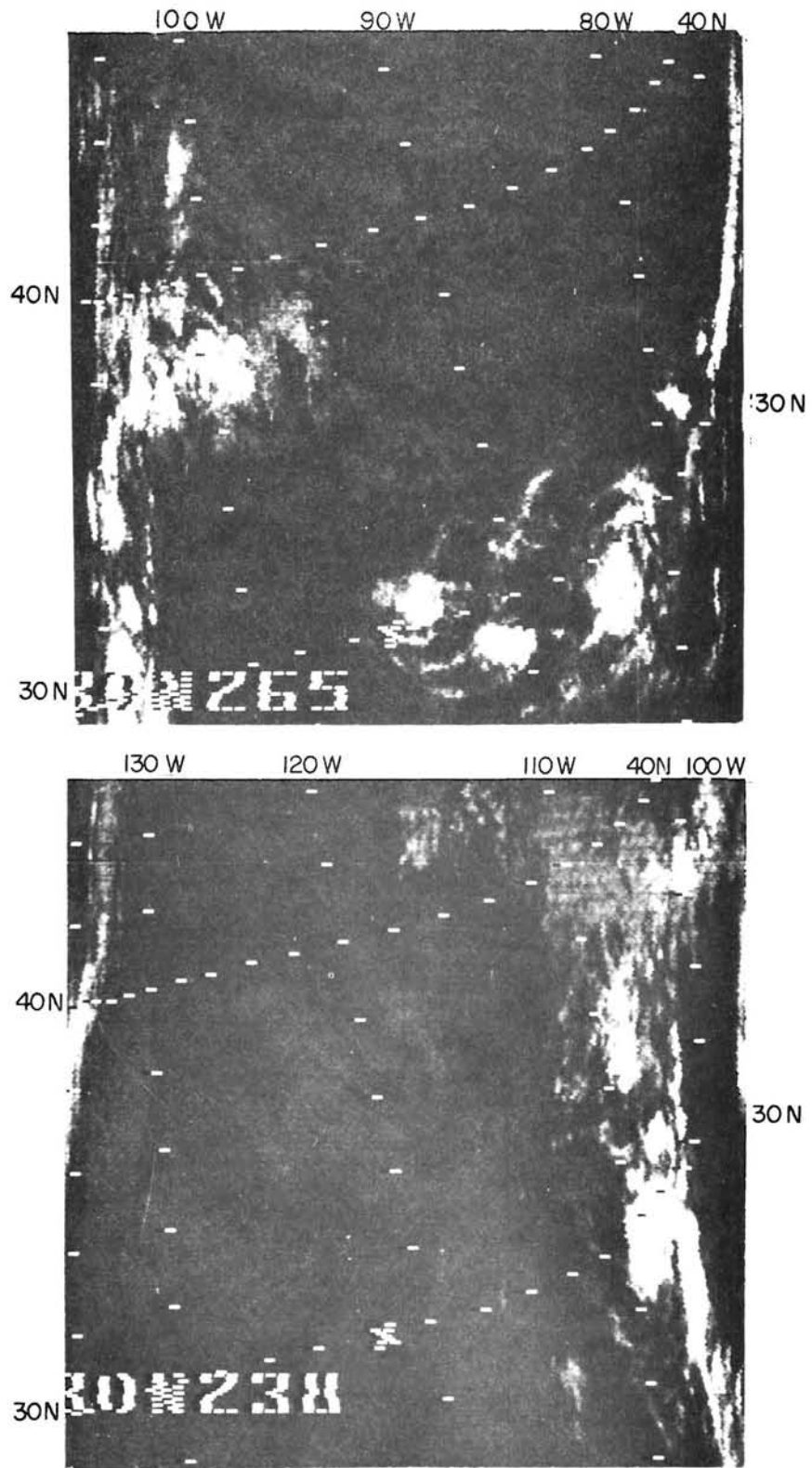


FIG. 5. Nimbus II HRIR, orbit 891 (upper) and orbit 892 (lower), 21 July 1966, approximately 0612 GMT and 0757 GMT.

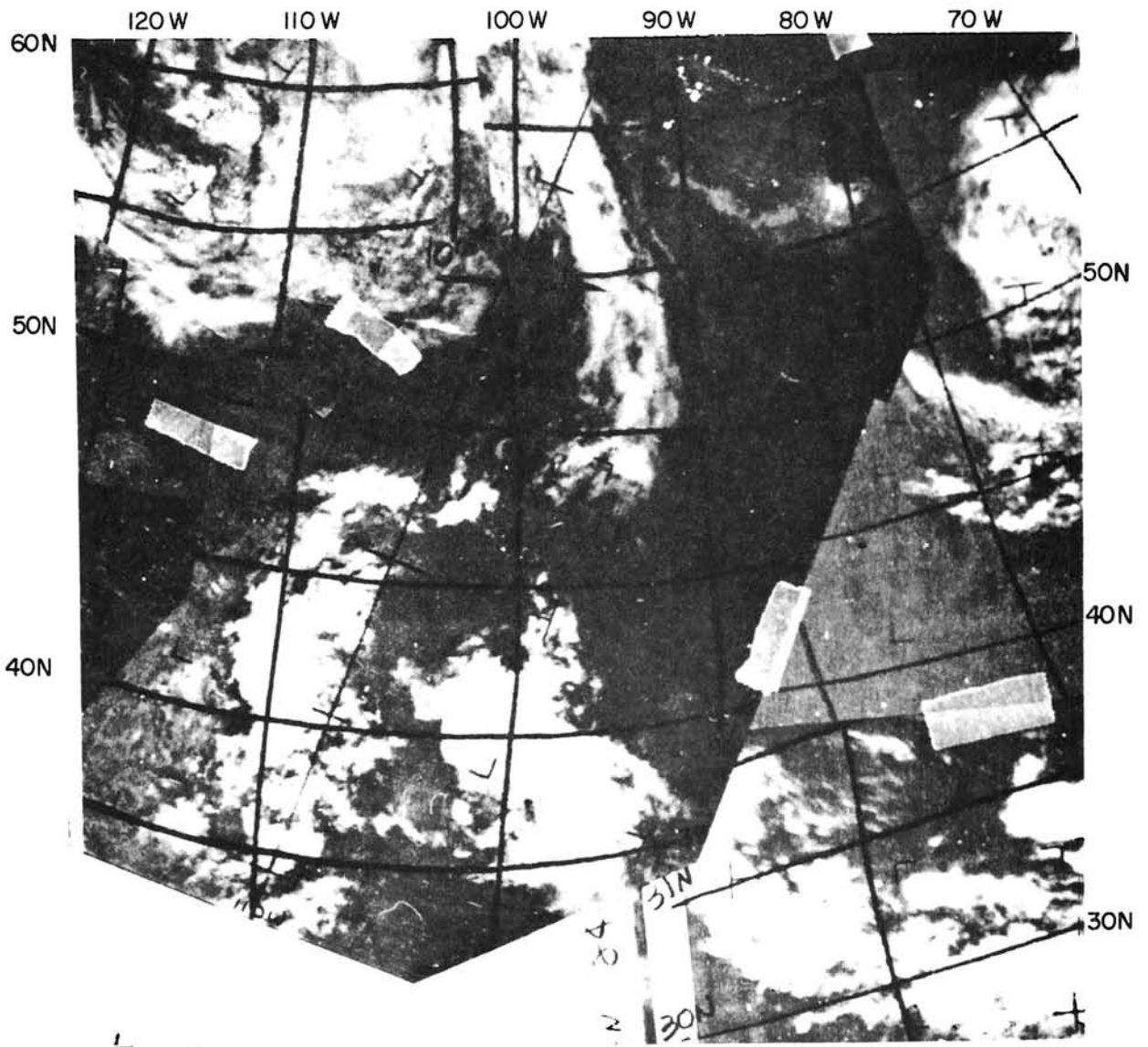


FIG. 6. ESSA II APT, composite, orbits 1815 and 1816, 21 July 1966, approximately 1431 GMT and 1616 GMT.

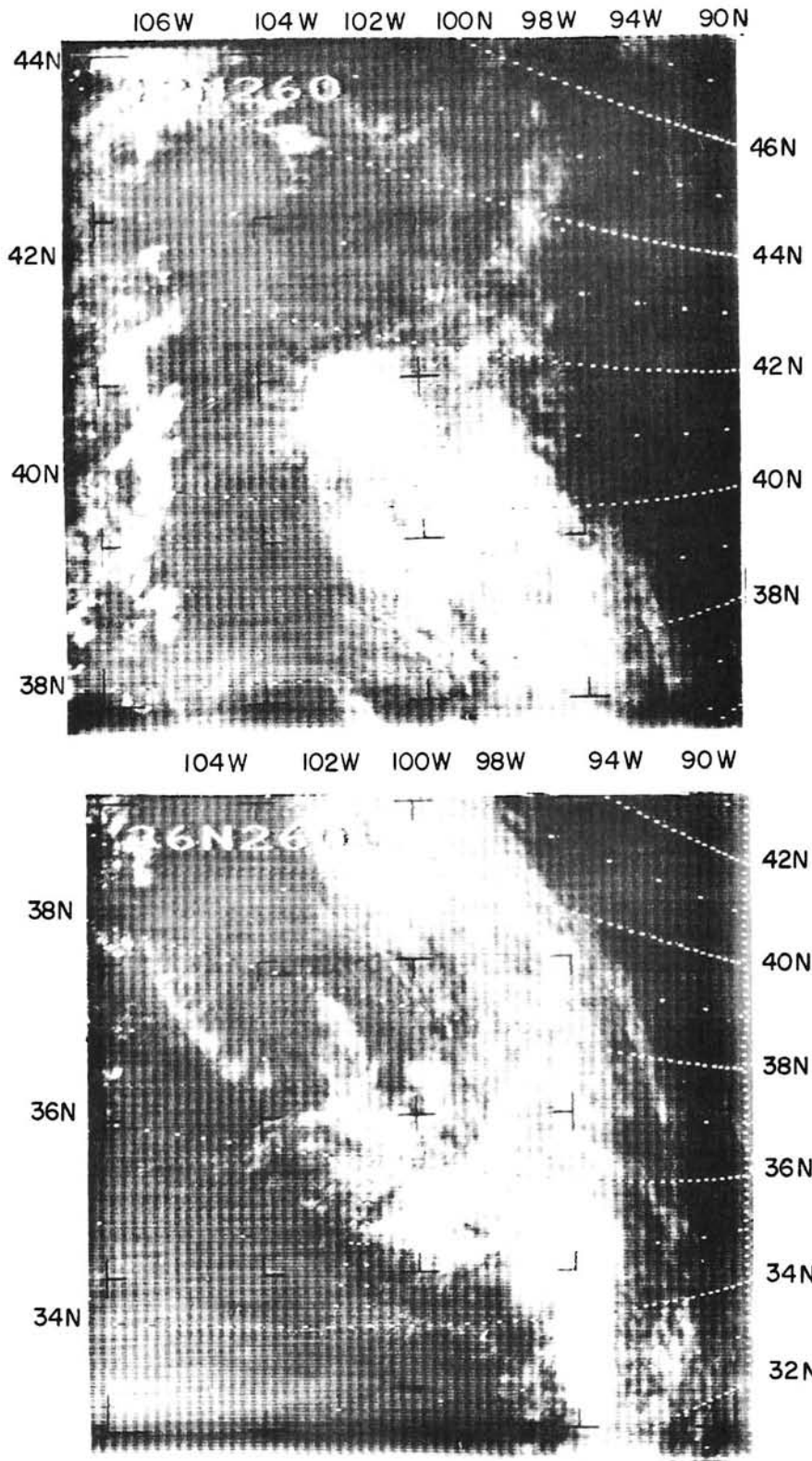


FIG. 7. Nimbus II AVCS, orbit 898, camera 3, frames 4 and 5, 21 July 1966, 1819 GMT.

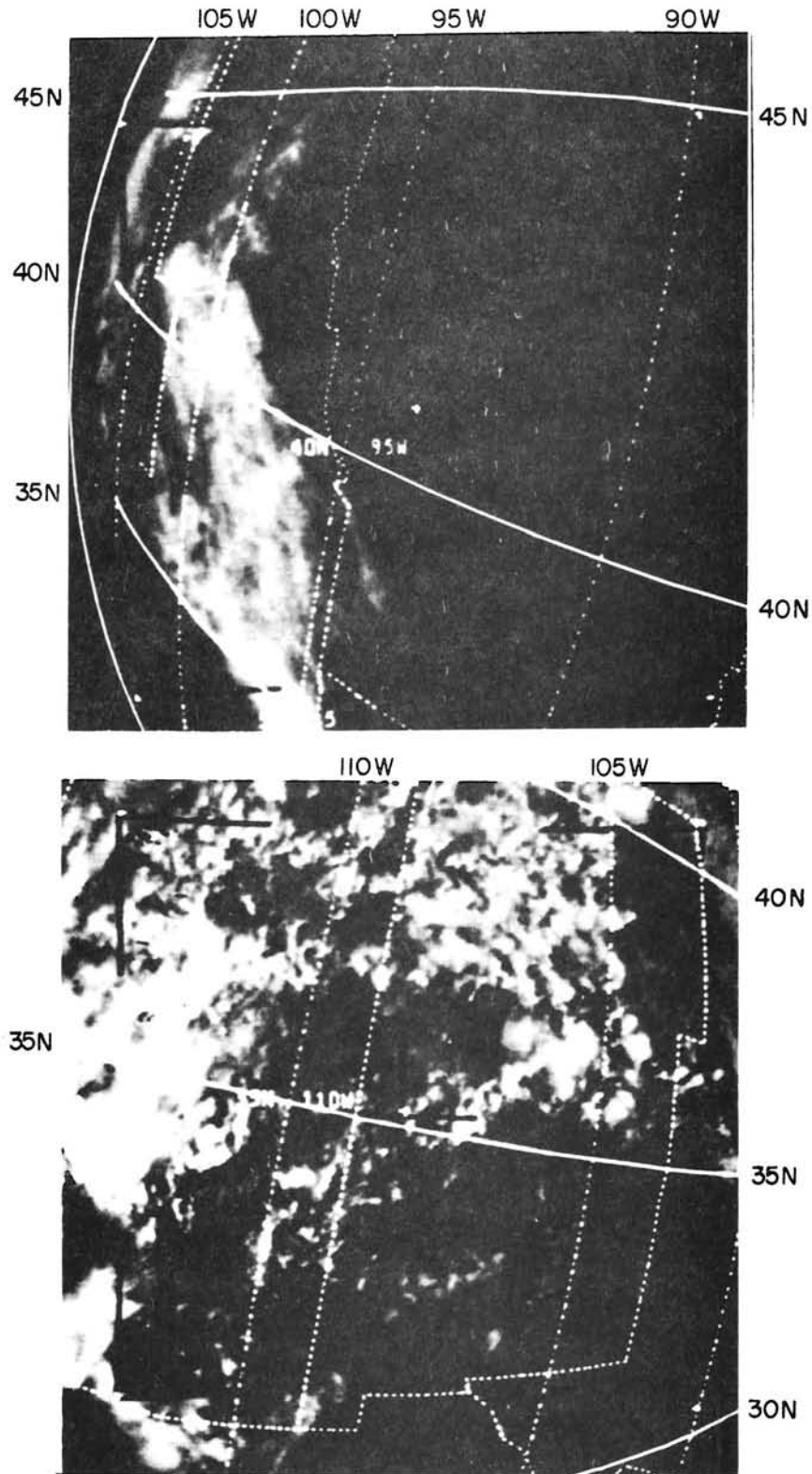


FIG. 8. ESSA I VCS, orbit 2417, camera 2, frame 3 (upper), and orbit 2418, camera 1, frame 4 (lower), 21 July 1966, 1900 GMT and 2038 GMT.

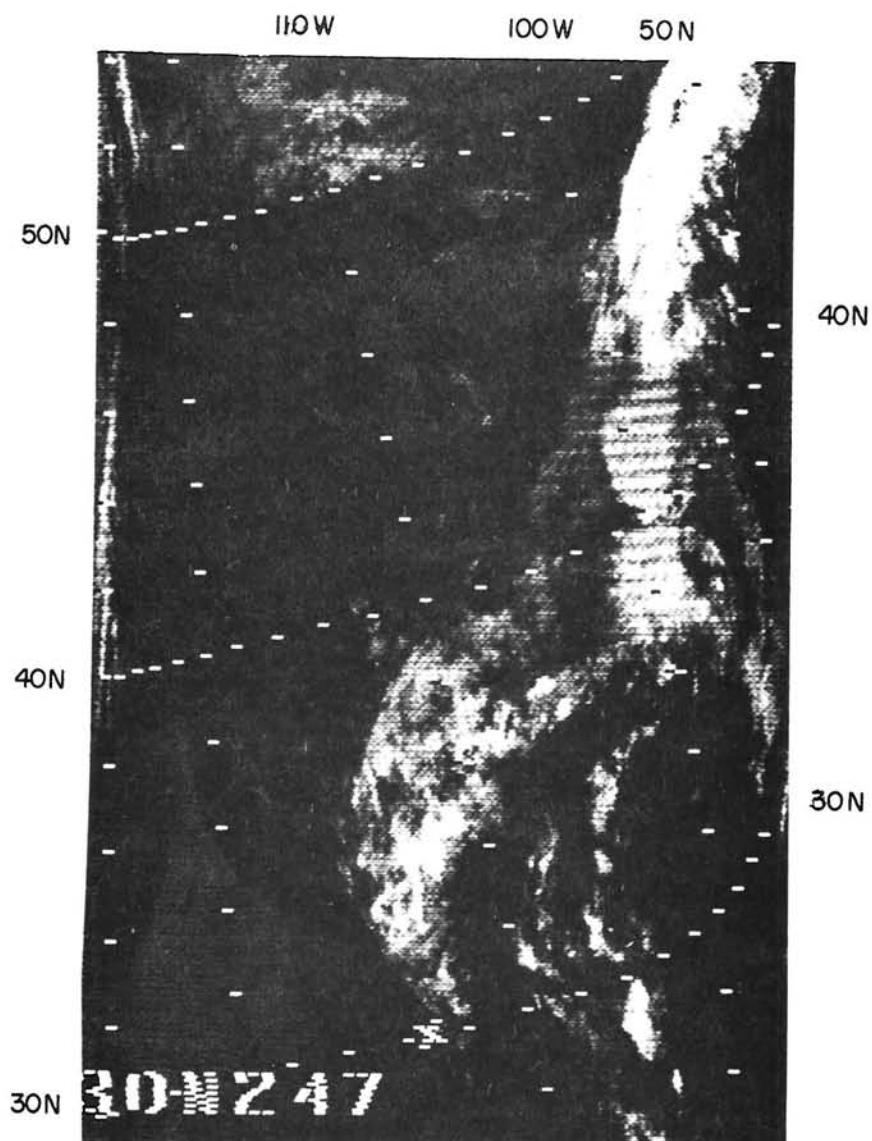


FIG. 9. Nimbus II HRIR, orbit 905, 22 July 1966, approximately 0724 GMT.

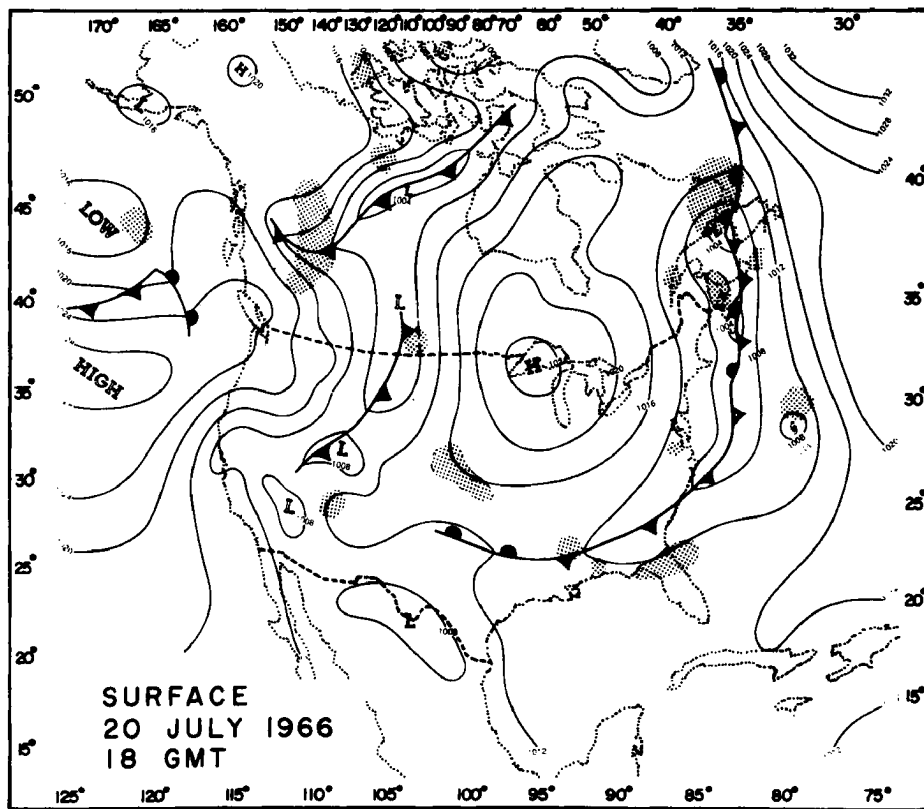
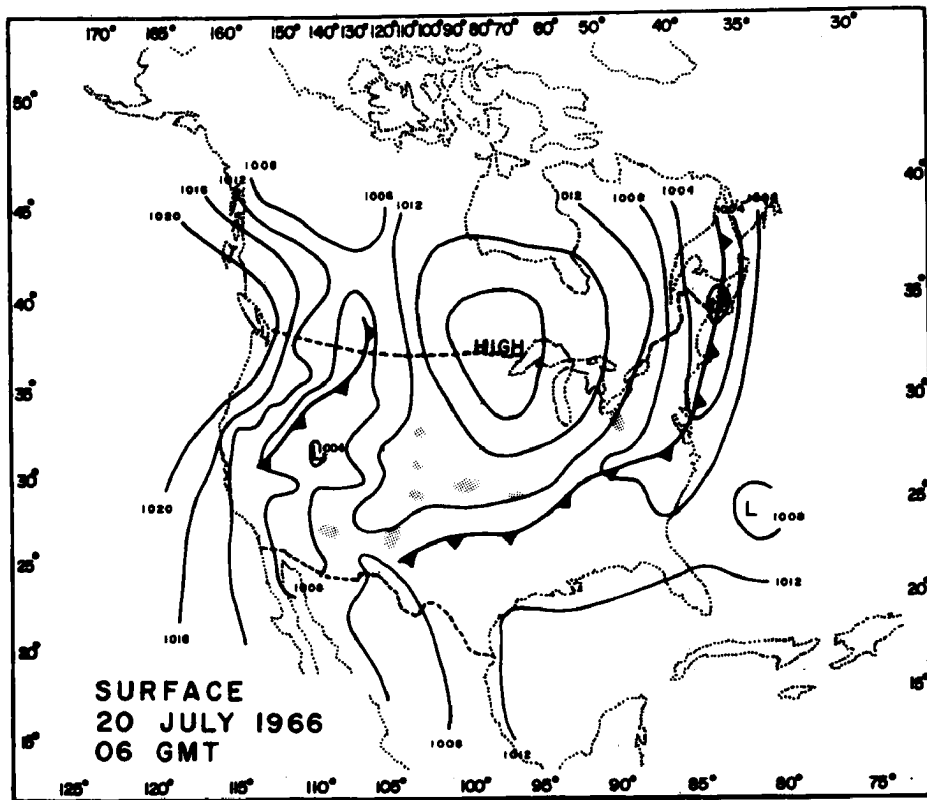


FIG. 10. Continued.

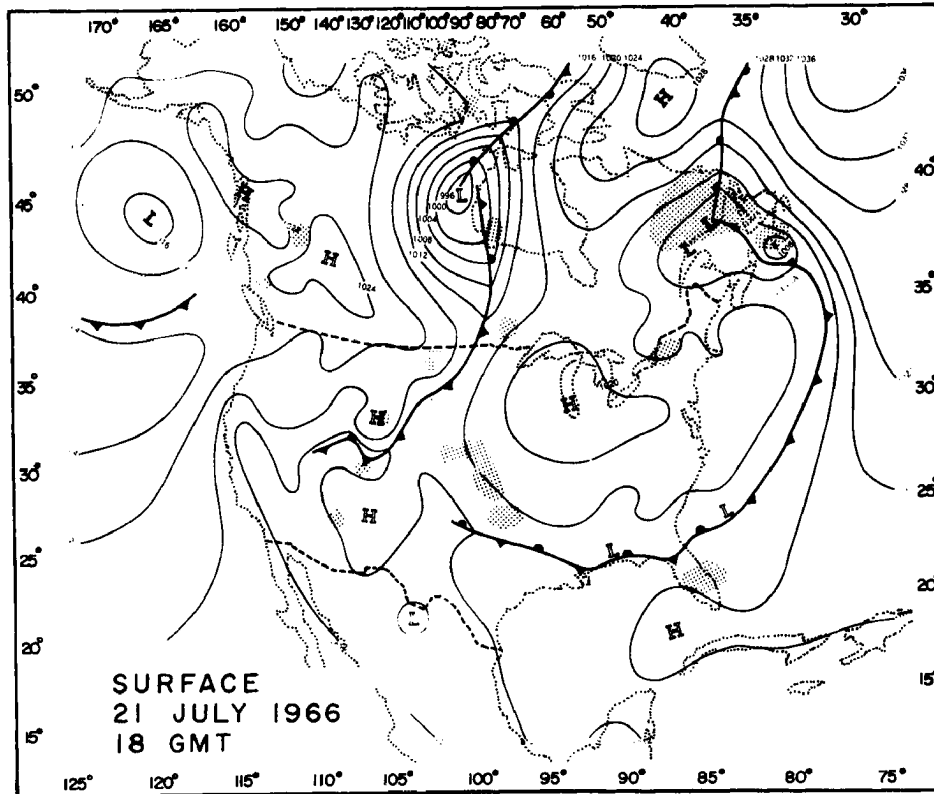
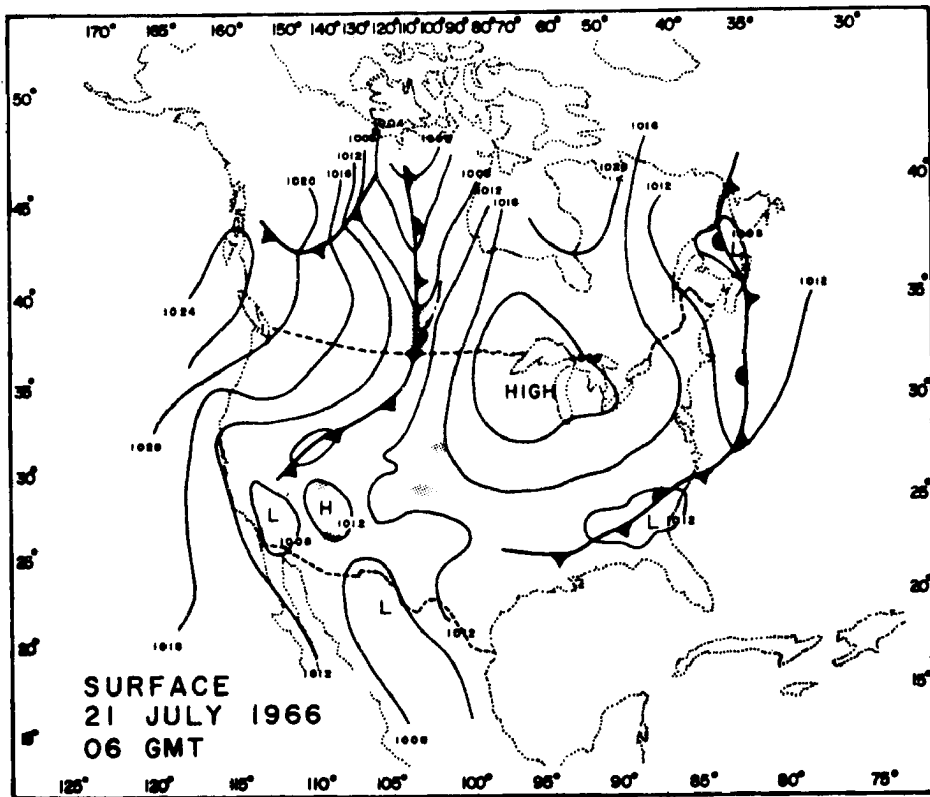


FIG. 10. Continued.

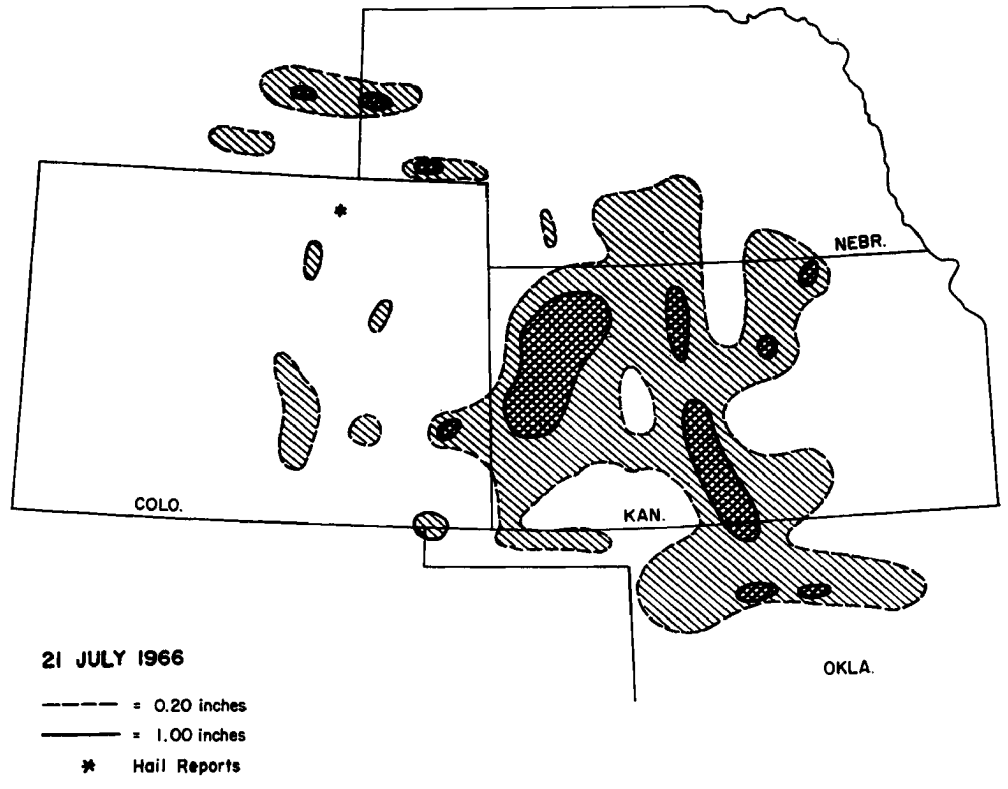
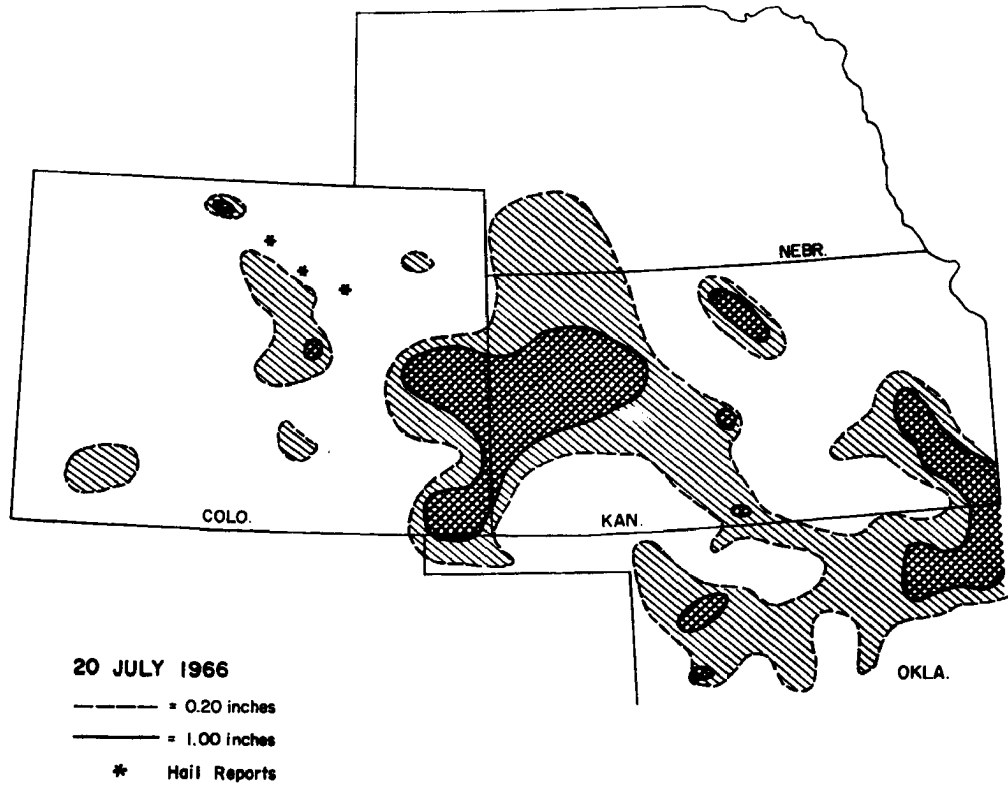


FIG. 11. Precipitation distribution and hail reports for 20 and 21 July 1966.

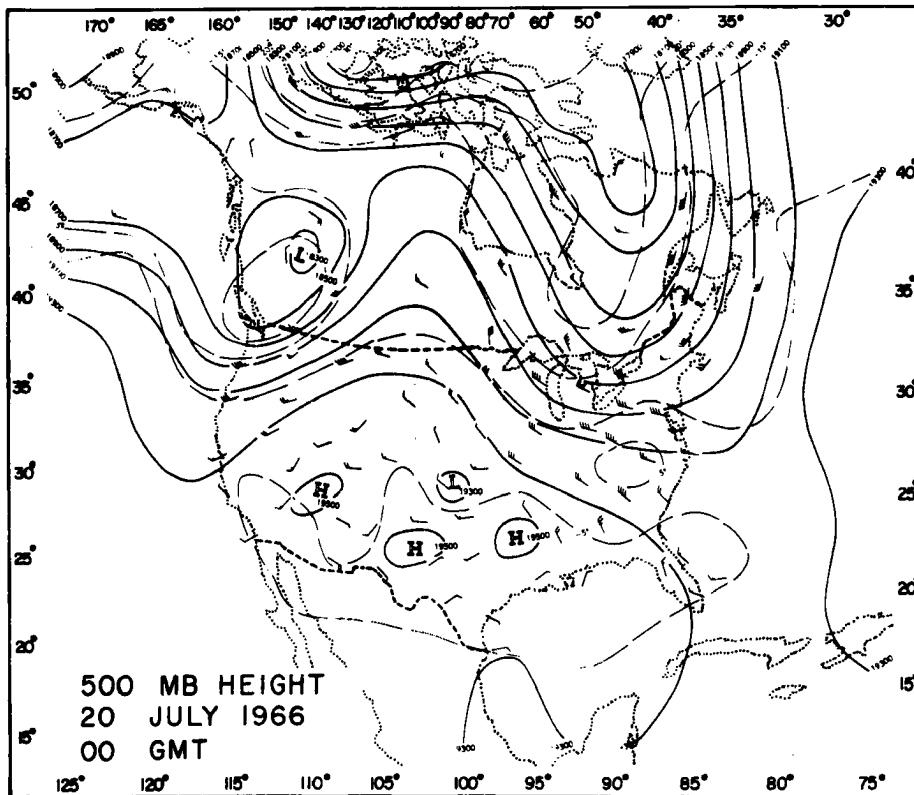
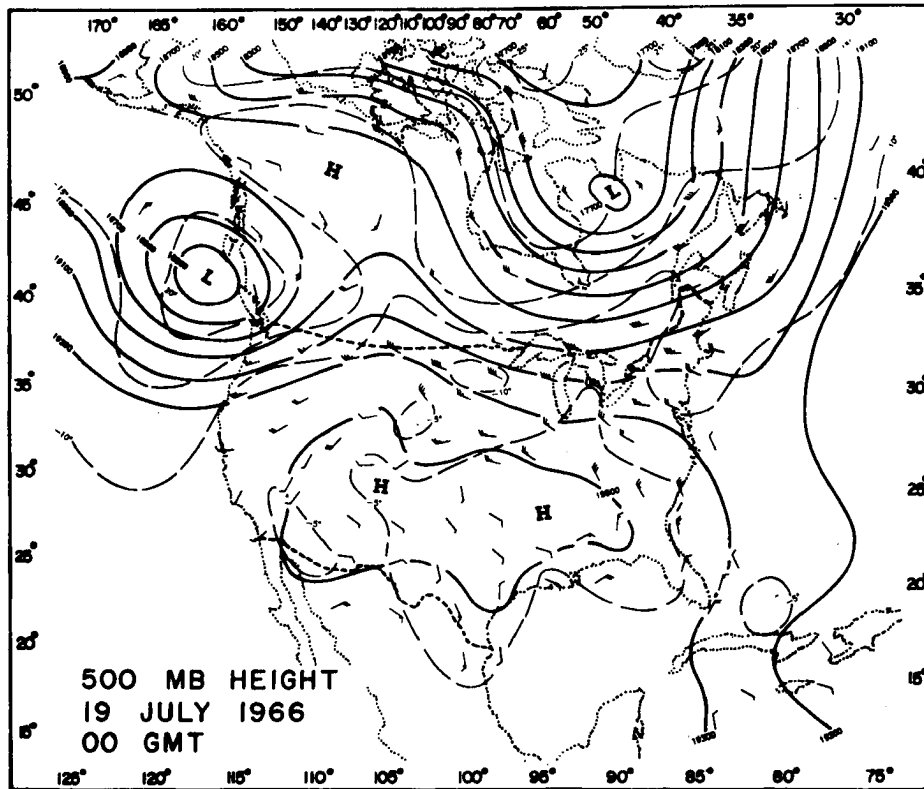


FIG. 12. 500 mb height contours (solid lines, in ft) for indicated times. Dashed lines are isotherms ( $^{\circ}\text{C}$ ). Arrows show wind direction and speed (knots). (Reproduced from: Daily Weather Map, U. S. Weather Bureau)

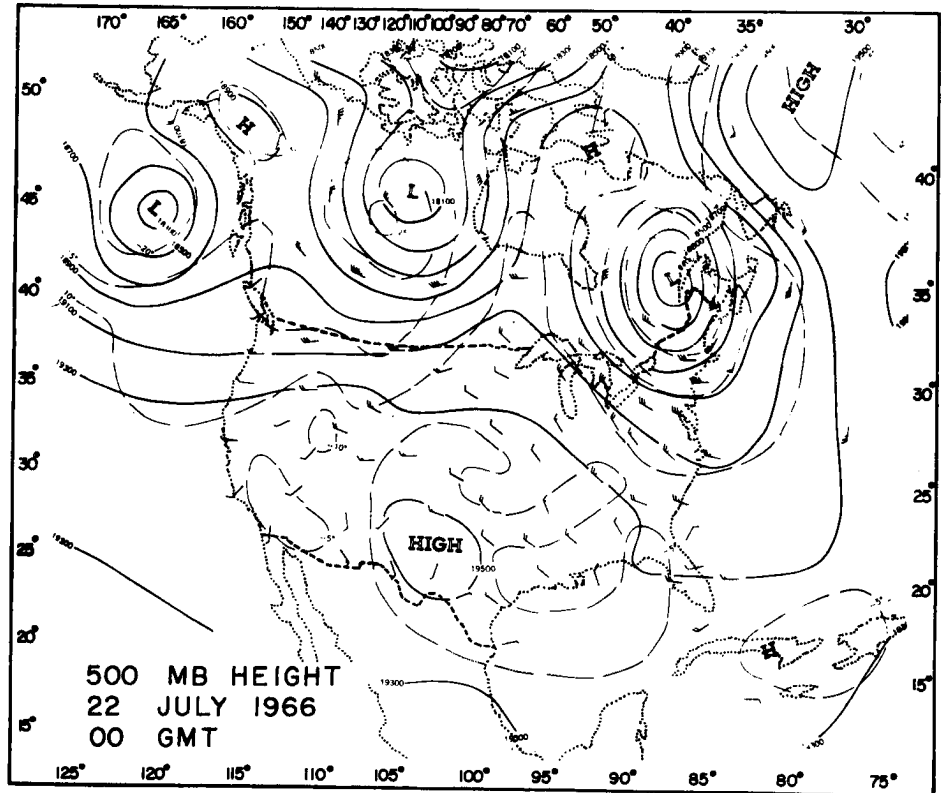
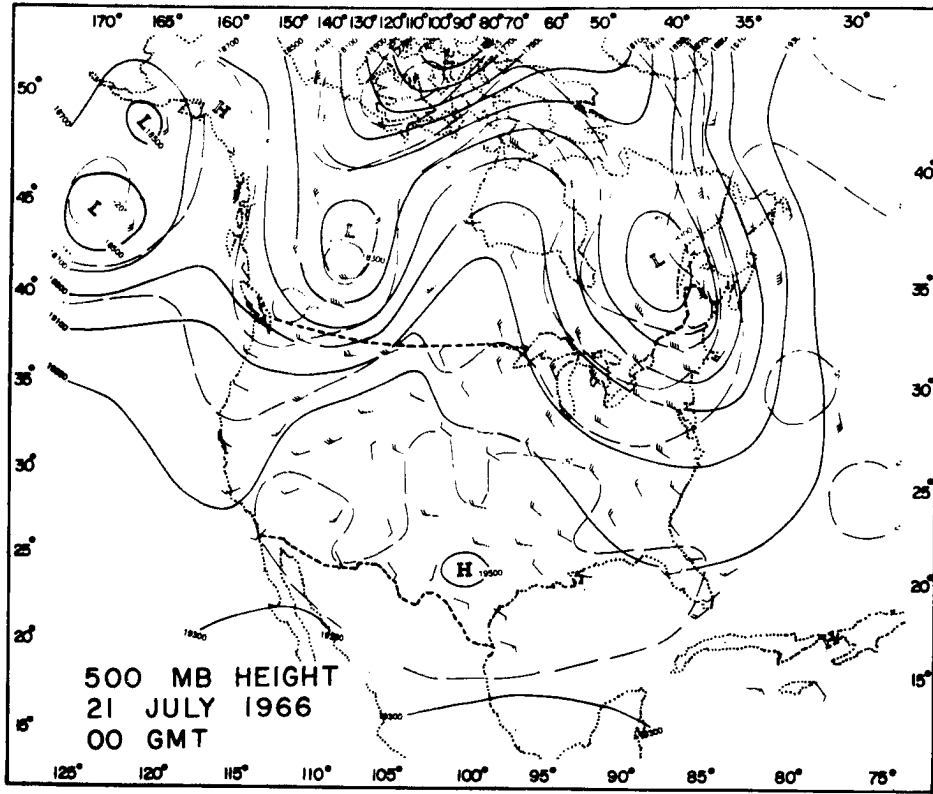


FIG. 12. Continued.

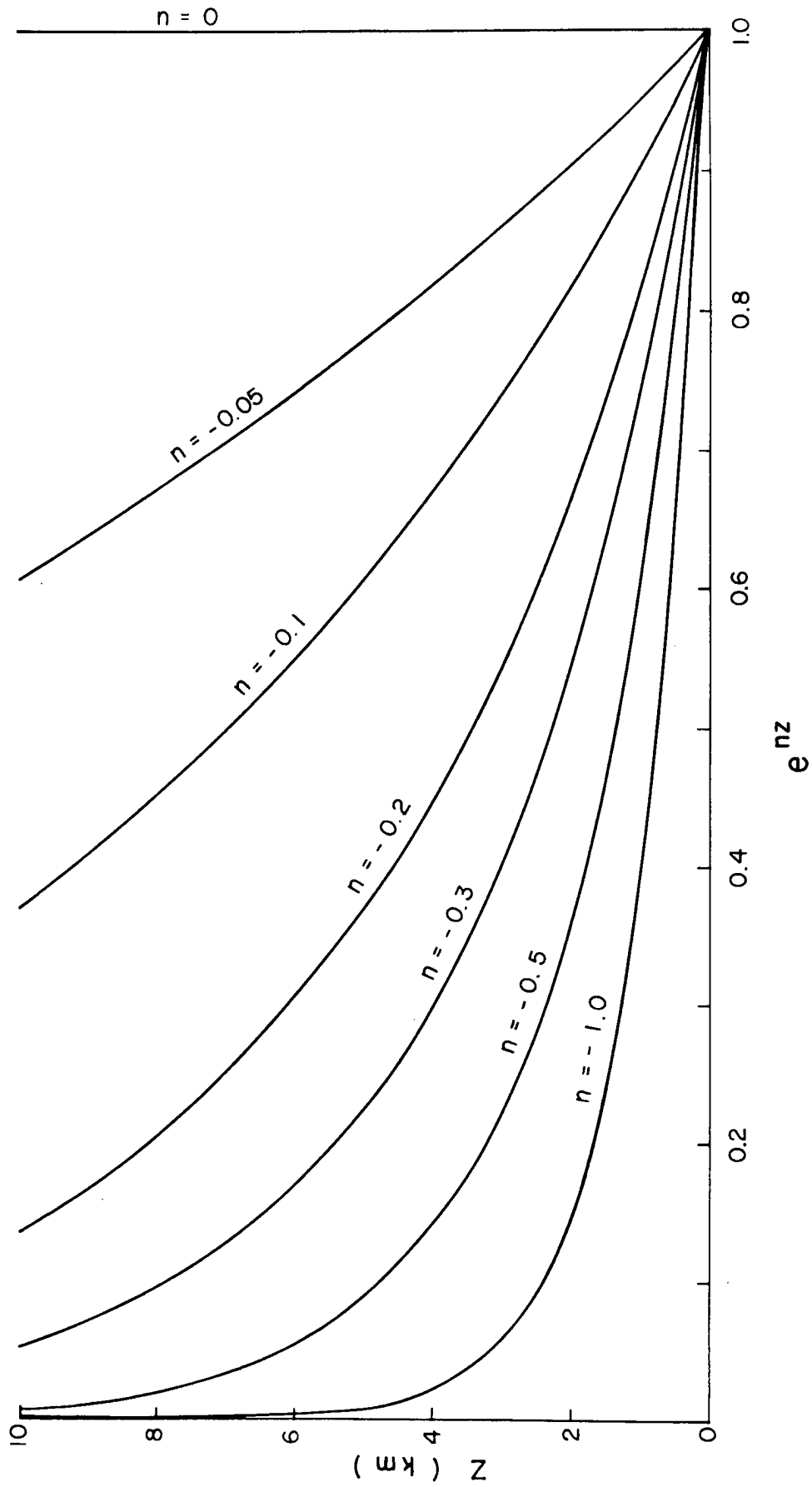


FIG. 13. Damping curves for various assumed values of  $n$  in the height range 0-10 km. Values of  $n$  are times  $10^{-3} \text{ m}^{-1}$ .

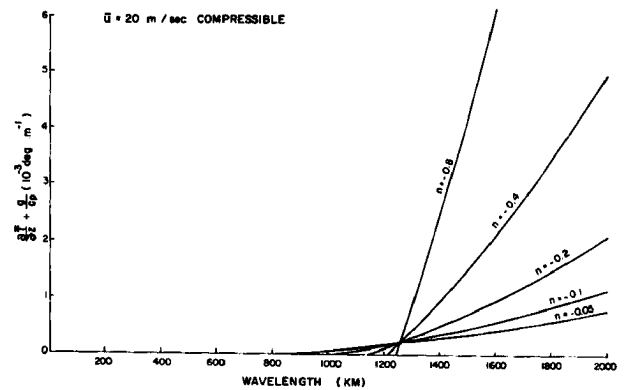
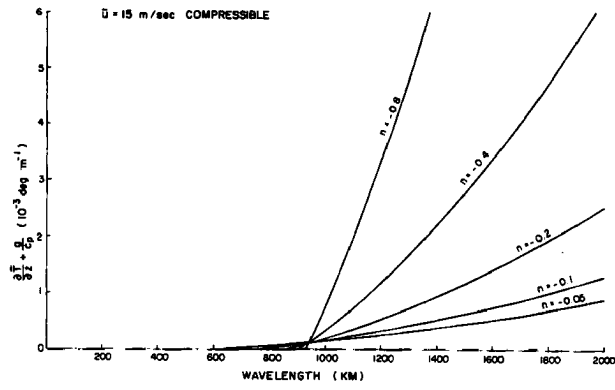
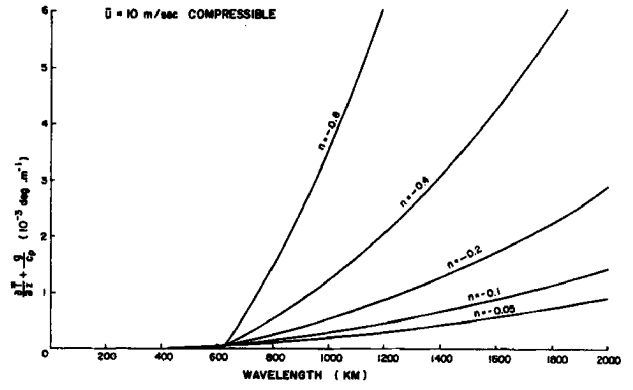
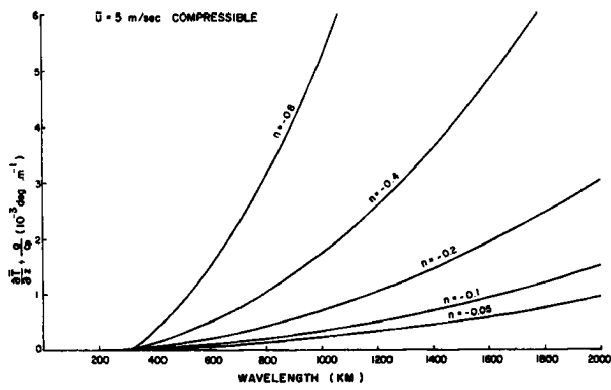


FIG. 14. Solutions of wavelength Eq. (24) for a compressible atmosphere as a function of various combinations of mean wind  $\bar{u}$  and damping coefficient  $n$ . Wavelength  $L$  is plotted against the stability  $\frac{\partial T}{\partial z} + \frac{g}{c_p}$ . Values of  $n$  are times  $10^{-3} \text{ m}^{-1}$ .

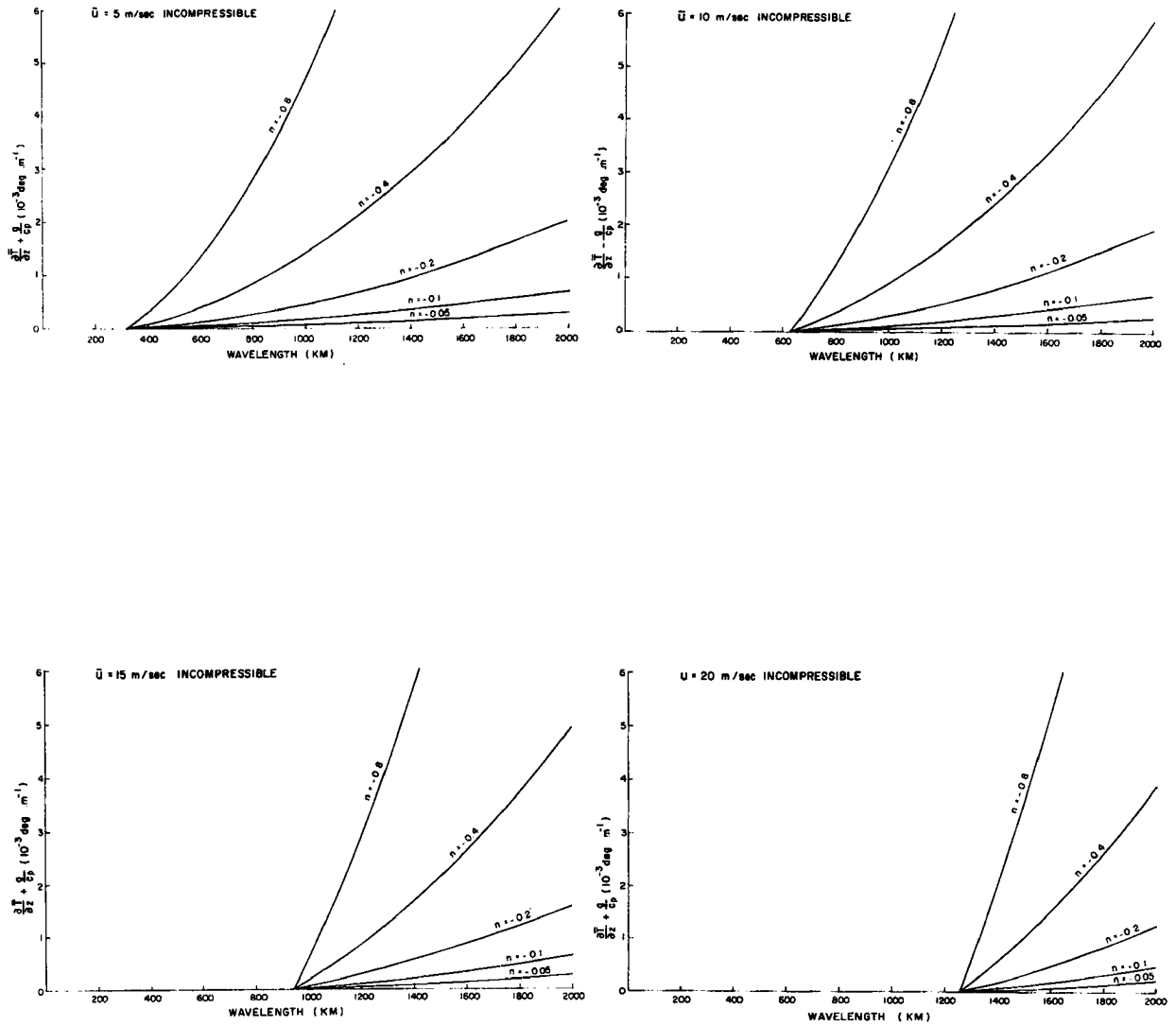


FIG. 15. Solutions of wavelength Eq. (24) for an incompressible atmosphere as a function of various combinations of mean wind  $\bar{u}$  and damping coefficient  $n$ . Wavelength  $L$  is plotted against the stability  $\frac{\partial T}{\partial z} + \frac{g}{c_p}$ . Values of  $n$  are times  $10^{-3} \text{ m}^{-1}$ .

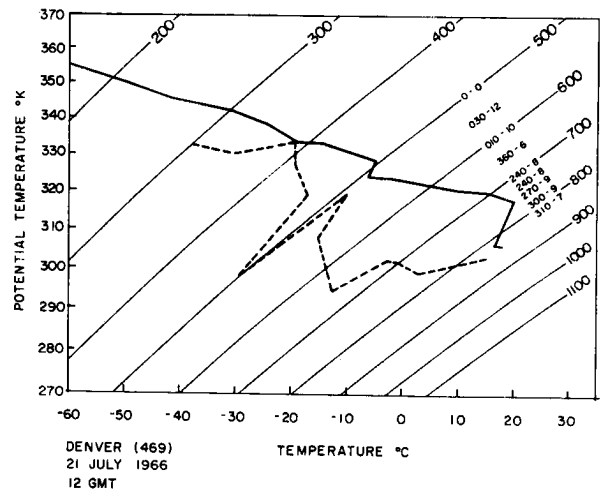
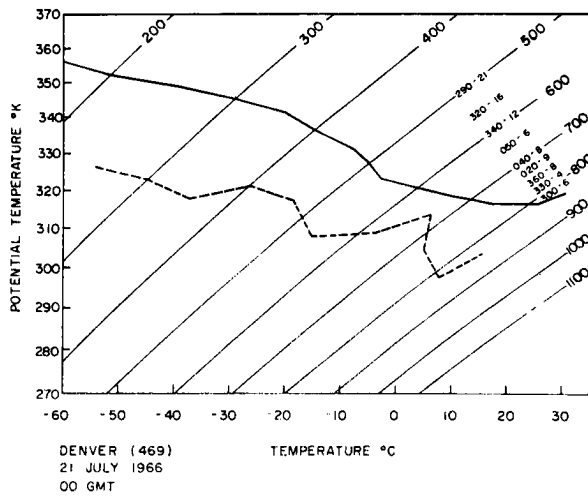
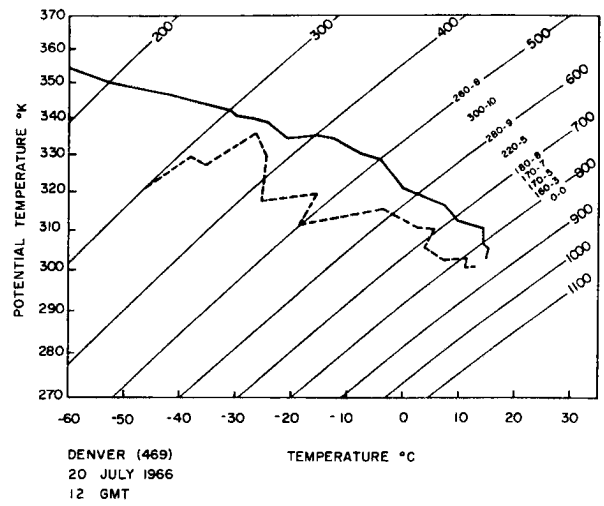
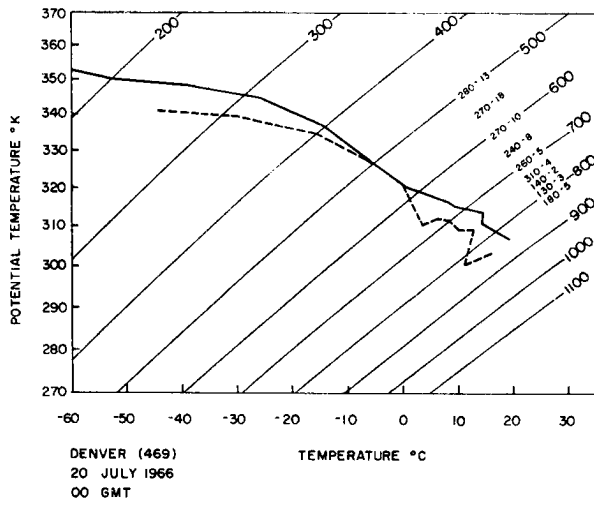


FIG. 16. Denver temperature soundings for indicated times plotted on a tephigram. Dew point sounding indicated by dashed line. Wind directions and speeds (knots) are plotted numerically along the sounding.

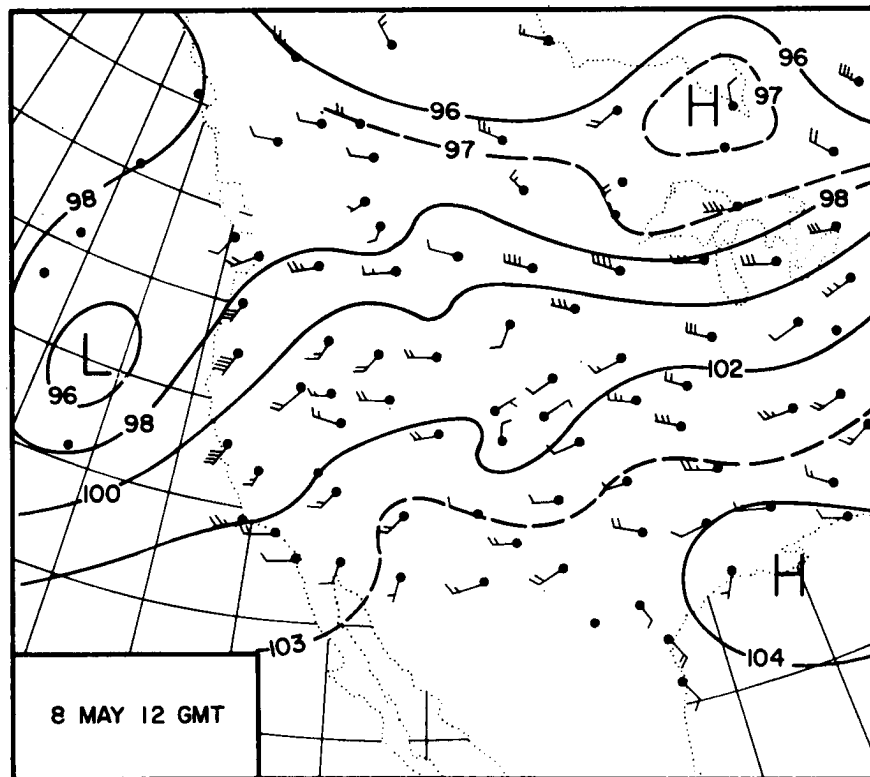
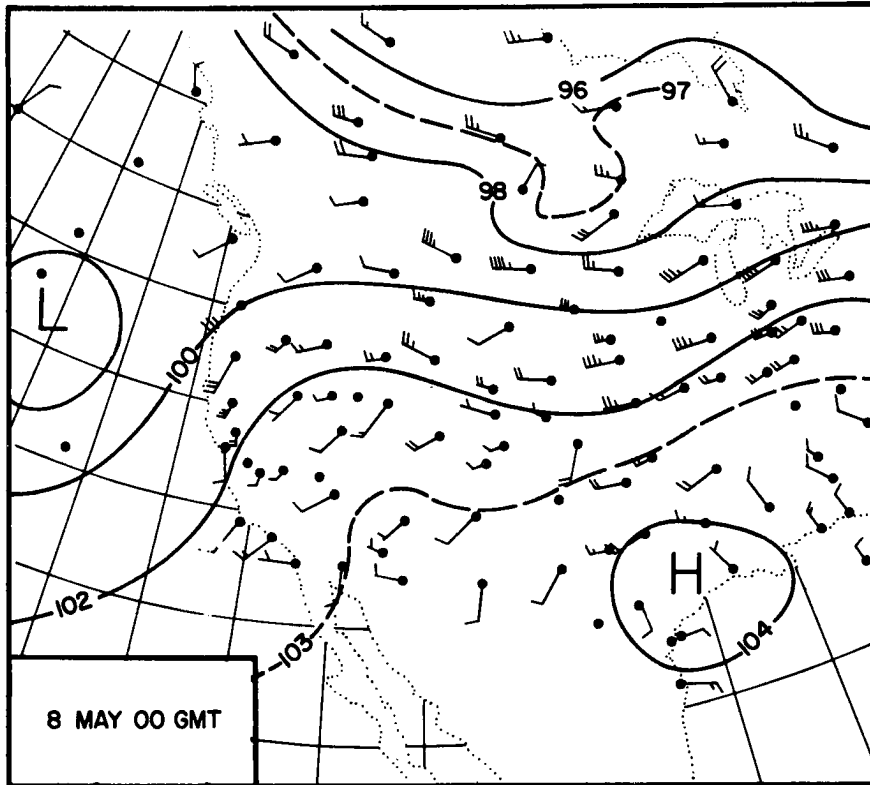


FIG. 17. 700 mb height contours (100 ft) for indicated times. Arrows show wind direction and speed (knots). (After Reiter and Mahlman, 1965)

Authors: R. A. Dirks, J. D. Mahlman  
and Elmar R. Reiter

551. 511. 3  
551. 515. 4

EVIDENCE OF A MESOSCALE WAVE PHENO-  
MENON IN THE LEE OF THE ROCKY MOUNTAINS

Subject Headings:  
Orographic Waves  
Mesoscale Systems

Colorado State University, Atmospheric  
Science Paper No. 115

Report under Grant E-10-68G from the National  
Environmental Satellite Center, ESSA

Satellite photographs during the summer months frequently reveal a weather situation in which strong convective development is observed over the Rocky Mountains and several hundred kilometers to the east of the mountains, while the region immediately to the lee is essentially cloud free. It is proposed that an orographically induced mesoscale wave phenomenon may produce this situation. A dynamical model is developed which yields standing wave solutions of wavelength < 1000 km for conditions of low mean wind speed and low thermal stability. Application of the model to the case of 20-21 July 1966 indicates a reasonable agreement between observation and theory; however, the sensitivity of the model to input parameters suggests that certain refinements need to be made.

Authors: R. A. Dirks, J. D. Mahlman  
and Elmar R. Reiter

551. 511. 3  
551. 515. 4

EVIDENCE OF A MESOSCALE WAVE PHENO-  
MENON IN THE LEE OF THE ROCKY MOUNTAINS

Subject Headings:  
Orographic Waves  
Mesoscale Systems

Colorado State University, Atmospheric  
Science Paper No. 115

Report under Grant E-10-68G from the National  
Environmental Satellite Center, ESSA

Satellite photographs during the summer months frequently reveal a weather situation in which strong convective development is observed over the Rocky Mountains and several hundred kilometers to the east of the mountains, while the region immediately to the lee is essentially cloud free. It is proposed that an orographically induced mesoscale wave phenomenon may produce this situation. A dynamical model is developed which yields standing wave solutions of wavelength < 1000 km for conditions of low mean wind speed and low thermal stability. Application of the model to the case of 20-21 July 1966 indicates a reasonable agreement between observation and theory; however, the sensitivity of the model to input parameters suggests that certain refinements need to be made.

Authors: R. A. Dirks, J. D. Mahlman  
and Elmar R. Reiter

551. 511. 3  
551. 515. 4

EVIDENCE OF A MESOSCALE WAVE PHENO-  
MENON IN THE LEE OF THE ROCKY MOUNTAINS

Subject Headings:  
Orographic Waves  
Mesoscale Systems

Colorado State University, Atmospheric  
Science Paper No. 115

Report under Grant E-10-68G from the National  
Environmental Satellite Center, ESSA

Satellite photographs during the summer months frequently reveal a weather situation in which strong convective development is observed over the Rocky Mountains and several hundred kilometers to the east of the mountains, while the region immediately to the lee is essentially cloud free. It is proposed that an orographically induced mesoscale wave phenomenon may produce this situation. A dynamical model is developed which yields standing wave solutions of wavelength < 1000 km for conditions of low mean wind speed and low thermal stability. Application of the model to the case of 20-21 July 1966 indicates a reasonable agreement between observation and theory; however, the sensitivity of the model to input parameters suggests that certain refinements need to be made.

Authors: R. A. Dirks, J. D. Mahlman  
and Elmar R. Reiter

551. 511. 3  
551. 515. 4

EVIDENCE OF A MESOSCALE WAVE PHENO-  
MENON IN THE LEE OF THE ROCKY MOUNTAINS

Subject Headings:  
Orographic Waves  
Mesoscale Systems

Colorado State University, Atmospheric  
Science Paper No. 115

Report under Grant E-10-68G from the National  
Environmental Satellite Center, ESSA

Satellite photographs during the summer months frequently reveal a weather situation in which strong convective development is observed over the Rocky Mountains and several hundred kilometers to the east of the mountains, while the region immediately to the lee is essentially cloud free. It is proposed that an orographically induced mesoscale wave phenomenon may produce this situation. A dynamical model is developed which yields standing wave solutions of wavelength < 1000 km for conditions of low mean wind speed and low thermal stability. Application of the model to the case of 20-21 July 1966 indicates a reasonable agreement between observation and theory; however, the sensitivity of the model to input parameters suggests that certain refinements need to be made.

ATMOSPHERIC SCIENCE PAPERS (Continued)

108. A General Computational Form for a Class of Nonlinear Systems Incorporating both Spectral and Finite Difference Approximations by F. Baer and R. L. King. Report prepared with support under Grant GA-761, National Science Foundation. February 1967.
109. Snow Crystal and Ice Nuclei Concentrations in Orographic Snowfall by E. E. Hindman II. Report prepared with support under Grant GP-4750, National Science Foundation. June 1967.
110. Further Studies on Atmospheric General Circulation and Transport of Radioactive Debris by J. D. Mahlman. Report prepared with support under Contract No. AT(11-1)-1340, U. S. Atomic Energy Commission. June 1967.
111. The Dependence of the Richardson Number on Scale Length by Elmar R. Reiter and Peter F. Lester. Report prepared with support under Grant WBG-59 from the National Environmental Satellite Center, ESSA. July 1967.
112. Radar Characteristics of Wintertime Storms in the Colorado Rockies by R. William Furman. Report prepared with support from the National Science Foundation, Grant No. GP-4750. July 1967.
113. On the Applicability of Silicon Cells in Atmospheric Radiation Studies by Inge Dirmhirn. Report prepared with support under Contract NGR-06-002-038 National Aeronautics and Space Administration. July 1967.
114. To be published at a later date.

The "Atmospheric Science Papers" are intended to communicate without delay current research results to the scientific community. They usually contain more background information on data, methodology, and results than would normally be feasible to include in a professional journal. Shorter versions of these papers are usually published in standard scientific literature.

Editorial Office: Head, Department of Atmospheric Science  
Colorado State University  
Fort Collins, Colorado 80521